# Directly Diode-Pump Ultrafast Lasers

Luís Miguel Fraga Dias
Mestrado Integrado em Engenharia Física
Departamento de Física e Engenharia
2021

**Orientador**
Prof. Dr. Helder Crespo, Prof. Associado, Dep. de Física e Astronomia
Fac. de Ciências

**Coorientador**
Dra. Rosa Romero, CEO, Sphere Ultrafast Photonics (Spin-off da U. Porto)

U.PORTO

FACULDADE DE CIÊNCIAS
UNIVERSIDADE DO PORTO

Todas as correções determinadas pelo júri, e só essas, foram efetuadas.

O Presidente do Júri,

Porto, _____/_____/_____

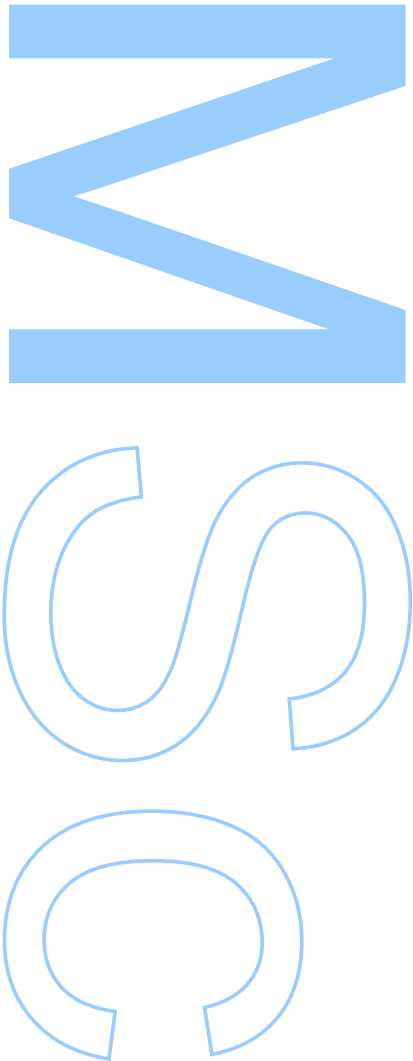

UNIVERSIDADE DO PORTO

MASTERS THESIS

# Directly Diode-Pump Ultrafast Lasers

*Author:*
Luís DIAS

*Supervisor:*
Dr. Helder CRESPO

*Co-supervisor:*
Dr. Rosa ROMERO

*A thesis submitted in fulfilment of the requirements*
*for the degree of MSc. Engineering Physics*

*at the*

Faculdade de Ciências da Universidade do Porto
Departamento de Física e Astronomia

December 21, 2021

*" Power's not an act, It's understanding truth, Changing my direction "*

Dream Theater - John Myung and John Petrucci

# *Acknowledgements*

I still can't believe that I'm here writing this. Reaching this milestone that is concluding a masters degree in Engineering Physics is something that when I entered in the physics department for the first time seemed so distant and, in a way, almost impossible that it doesn't even feel real. But it is!

These were definitely the most intense and tough years of my life where throughout the many challenges that the degree showed I really had to push forward my learning, working and thinking skills. But they were also the best ones where I got to share many incredible experiences with all the people that surrounded me and where I really feel that I evolved as a human being and as a person that loves science.

This thesis is a culmination of a lot of hard work, persistence and learning and its realization would not be possible without the guidance and expertise of many people. To this people and to all my family and friends I would like to present my sincere acknowledgements.

To my supervisor, Dr. Helder Crespo, I would like to thank for all the guidance and knowledge and also for revising this thesis.

To my co-supervisor, Dr. Rosa Romero, I would like to thank for all the guidance, knowledge, help during my time at Sphere Ultrafast Photonics and for revising this thesis.

To Dr. Miguel Canhota I would like to thank for accompanying me during my time at FEMTOLAB, for the huge help through the process of pumping the Ti:Sapphire oscillator and for revising this thesis. To all the people at FEMTOLAB, namely Dr. Ana Vieira Silva, Ana Oliveira e Silva, Tânia Ribeiro, Tiago Gomes and Dr. Tiago Mgalhães I would also like to thank for creating an awesome working environment.

To all the people at *Sphere Ultrafast Photonics*, namely Dr. Paulo Guerreiro, Dr. Miguel Miranda, Dr. Vítor Amorim, João Rodrigues, Luísa Cruz and Ricardo Moreira, I would also like to thank for all the patience, guidance and knowledge. It was very motivating to work around such incredible people.

To Bruno Jarrais I would like to thank for all the help with the measurements of the mirrors' transmittance.

To all my friends at FCUP I would like to thank for all the fun, happy and stressful moments throughout this five awesome years. You are the best! A special thanks to Rita Bugalhão for just being an incredible human being, for all the help and for being the

absolute best friend and group mate ever, to Carlos Callaty for being an awesome friend, for all the cool conversations about music and for all the concerts we've seen together and to Bruno Mota for all the memories that we share together. You're a brother to me!

To all my band mates at Phase Transition, namely Sofia Beco, Fernando Maia and José Pereira, and at Moonshade, also Fernando Maia, Pedro Quelhas, Ricardo Pereira, Nuno Barbosa and Sofia Hdz (yes, for me you're part of the band), I would like to thank for all the amazing experiences we have been through together and for being part of one of the things I love the most - music. Life is not just physics and the moments I shared with you until now have taught me valuable lessons that will always be helpful for both my personal and professional life.

Also in the context of music I would also like to thank to Luís Pinto for all the knowledge and life lessons. You are the best friend and music teacher one could have.

To my parents, Beatriz Dias and José Dias, and sister, Ana Fraga, I would like to thank for all the love, patience and support. I am the happiest and luckiest son and brother in the world for having the best family ever. This thesis would not be possible without you so I thank you the most.

Finally, to Beatriz Moreira I would like to thank for everything. For always being there, for talking with me, for calling me to reason in the stressful moments, for making me happy, for being the best human being that exists and, especially, for existing in my life. I love you.

UNIVERSIDADE DO PORTO

# *Abstract*

Faculdade de Ciências da Universidade do Porto
Departamento de Física e Astronomia

MSc. Engineering Physics

**Directly Diode-Pump Ultrafast Lasers**

by Luís DIAS

In this work we built, characterized and designed an optical system based on a blue laser diode (470 nm at 2.57 A and with an optical output power of 2.435 W) for directly pumping a Ti:Sapphire oscillator.

We started with the electrical characterization of the driver (PCB) in order to verify whether or not it was safe to connect it to the laser diode since these are very sensitive to electrostatic discharge. Measurements of the transient behaviour and all the outputs of the circuit board were performed, concluding that it was safe to connect the laser diode to it. In order to characterize the diode we made a plot of the output optical power as a function of time and measured its spectrum, concluding that it had a peak emission wavelenght at 470 nm with a constant output optical power of 2.435 W, corresponding to an electrical current of 2.57 A.

In the second half of this work we designed a collimation and astigmatism compensation system for the laser diode. We started by simulating the beam's propagation along a calculated optical system based on a combination of one meniscus lens and two cylindrical lenses in a telescopic configuration. Then we acquired the lenses and aligned the system so that, at the end, we had a pumping system based on a laser diode with the needed characteristics for pumping a Ti:Sapphire oscillator. After this process we proceeded with the pumping of the Ti:Sapphire oscillator stage which encompassed the alignment of the oscillator, the characterization of a DPSS laser (our reference pump source) and the pump mirrors, and the $P_{out}$ vs $P_{pump}$ graph for this DPSS laser as the pump source. We also compared the beam of our laser diode to the DPSS one in order to see how good our developed pump source is in comparison with the reference one.

UNIVERSIDADE DO PORTO

# *Resumo*

Faculdade de Ciências da Universidade do Porto
Departamento de Física e Astronomia

Mestrado Integrado em Engenharia Física

**Lasers Bombeados Diretamente por Díodos**

por Luís DIAS

Neste trabalho construímos, caracterizamos e projetamos um sistema óptico baseado num díodo laser azul (470 nm a 2,57 A e com uma potência ótica de saída de 2,435 W) para bombeamento de um oscilador Ti:Safira.

Começamos pela caracterização elétrica da fonte de corrente estabilizada (*driver* PCB) para verificar se era ou não seguro conectá-la ao díodo laser, dado estes serem muito sensíveis a descargas eletrostáticas. Foram realizadas medições do comportamento transiente em todas as saídas da placa de circuito impresso, concluindo que era seguro ligar o díodo laser. Para a caracterização do díodo, fizemos um gráfico da potência ótica de saída em função do tempo e medimos o seu espetro, concluindo que este tem um comprimento de onda de emissão de pico em 470 nm com uma potência ótica de saída constante de 2,435 W, correspondente a uma corrente elétrica de 2,57 A.

Na segunda metade deste trabalho construímos um sistema de colimação e compensação de astigmatismo para o díodo laser. Começamos por simular a propagação do feixe ao longo de um sistema óptico previamente calculado baseado na combinação de uma lente menisco e duas lentes cilíndricas em configuração telescópica. Em seguida, adquirimos as lentes e alinhamos o sistema de forma a que, no final, tivéssemos um sistema de bombeamento baseado num diodo laser com as características necessárias para bombear um oscilador Ti:Safira. Após este processo, prosseguimos para a fase de bombeamento do oscilador Ti: Sapphire que englobou o alinhamento do oscilador, a caracterização de um laser DPSS (a nossa referência como fonte de bombeamento) e dos *pumping mirrors*, e o gráfico $P_{out}$ vs $P_{bomba}$ para este laser DPSS como fonte de bombeamento. Além disto também comparámos o feixe do nosso diodo laser em relação ao do DPSS para ver o quão boa é a nossa fonte de bombeamento em comparação com a de referência.

# Contents

# List of Figures

*This thesis is dedicated to my parents and sister for all the love, patience and support throughout the years.*

# Chapter 1

# State of the art

Semiconductor lasers have become widespread not only because they can be implemented in a variety of applications and are relatively cheap comparing with other types of lasers, but also because they are very reliable as pump sources for solid state lasers and lasers in general for both pulsed and continuous modes of operation. Basically, these lasers work by the principle of stimulated emission of radiation at an interband transition in the active medium when the energy of transition is larger than the band-gap. The active medium is generally composed of a combination of elements from the Group III (Al, Ga and In, for example) and elements from the Group V (N, As and Sb, for example) of the periodic table forming alloys such as GaAs, AlGaAs, InGaAs and InGaAsP [1].

This technology was firstly idealized by *Basov* et al. (1961) [2] when he proposed that stimulated emission of radiation could happen by recombination of carriers in *p*-*n* junctions. The following year (1962) laser action in a semiconductor was first observed in three different laboratories. At the time these devices were being developed with the same material (GaAs) for both the *p* and *n* sides of the junction which we now call homojunction lasers. Unfortunately, these lasers can only operate in continuous wave (cw) mode at cryogenic temperatures which makes them unusable for most applications. It was only 7 years later (1969) that heterojunction lasers were invented which has enabled semiconductor lasers at room temperature, making the homojunction only of historical importance. The difference between a homostructure and a heterostructure semiconductor laser is that the first has a junction made of materials with the same band-gap (usually the same materials) and the latter has a junction made of materials of different band gaps (usually different materials) [2].

## 1.1 Semiconductor Laser Operation - Fundamentals

Semiconductor lasers, as previously explained, can amplify light by exploring transitions between the valence and the conduction band in the active medium of the *p-n* junction but before starting to explain this phenomena, it is important to overview some key solid-state principles like band structure, band gaps and *p* and *n* doped media.

***Band structure*** - electrons of an isolated atom occupy atomic orbitals with discrete energy levels. When an atom combines with another to form a molecule each atomic orbital splits to form two new orbitals with different energy states because, as Pauli's exclusion principle dictates, two electrons with the same quantum numbers cannot be in the same atomic orbital. When there are $N$ atoms in a structure ($N$ usually being $10^{22}$ order of magnitude) the atomic orbitals will split into $N$ closely spaced new orbitals with different energy states, forming a band. This only happens to the outermost electrons (the valence and conduction electrons) because the innermost ones are too strongly attached to the nucleus for their atomic orbitals to overlap with another atom's innermost electrons.

***Band gap*** - band gap is the energy spacing between different bands where there is no electronic states. We can visualize a material's conducting properties by their band gap between the valence and the conduction bands as demonstrated in figure 1.1:

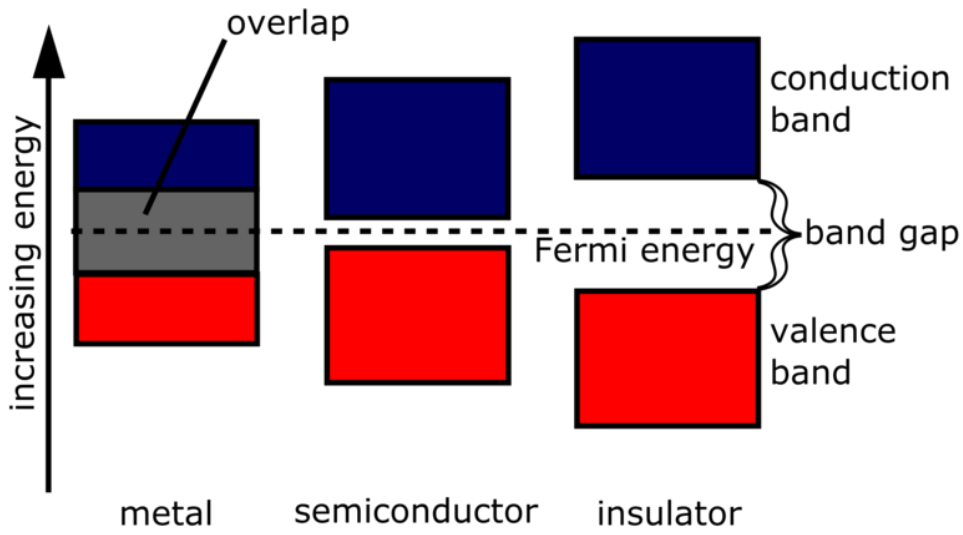


FIGURE 1.1: Band Gap [3]

As we can see, an insulator has a huge band gap which makes transitions between the valence band to the conduction band very difficult for electrons. That is why this kind of

materials have no conducting properties (at ordinary temperatures) unless the temperature gets very high (this usually destroys the material). On the other side, materials like metals are very good conductors because their valence and conduction bands overlap. In the middle side of the spectrum we have semiconductors, whose band gaps are small enough for them to have great conducting properties (especially when they are doped) and big enough for not being considered conductors.

***Doped media*** - to improve the conducting properties of semiconductors, as previously said, it is common to dope them with impurities that will create energy states within the valence and conduction bands. When we dope a semiconductor with electron-donor impurities ($n$ doping) we are creating energy states in the conduction band and when we dope it with electron-acceptor ones ($p$ doping) we are creating energy states in the valence band. Moreover, if we dope a material with $p$ and $n$ impurities a semiconductor junction is created at the interface.

To begin the exploration of the semiconductor lasing concept, let's consider a basic two band system (one valence band and one conduction band) separated by the band gap energy $E_g$ before and after the pumping process, as demonstrated in 1.2:

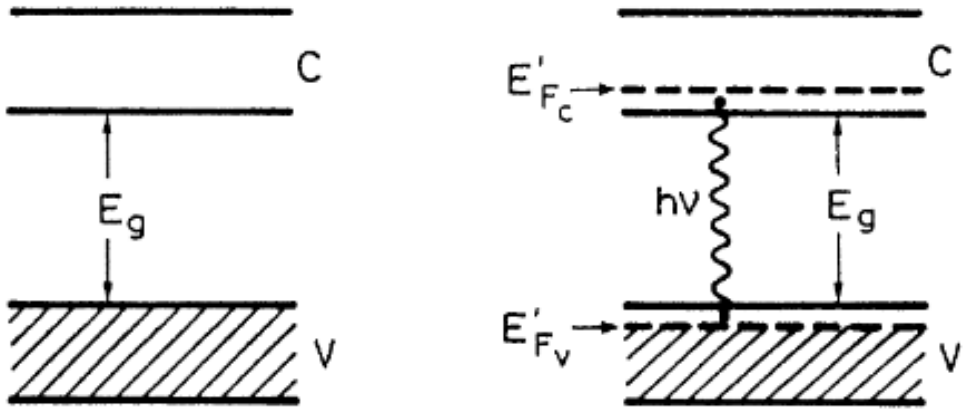


(A) System before pumping. (B) System after pumping.

FIGURE 1.2: Two band system at $T = 0$ K [1]

We can see by the hatched area that, before the pumping process, the valence band is completely filled. By stimulating the valence electrons with some pumping process we can make them transit to the conduction band provided we excite them with a photon with more energy than the band gap. $E'_{F_c}$ and $E'_{F_v}$ represent, at $T = 0$K and for each band, the energy below which states are fully occupied by electrons and above which,

states are empty. The energy states within the medium can be visualized by plotting **E vs k** in the parabolic approximation.

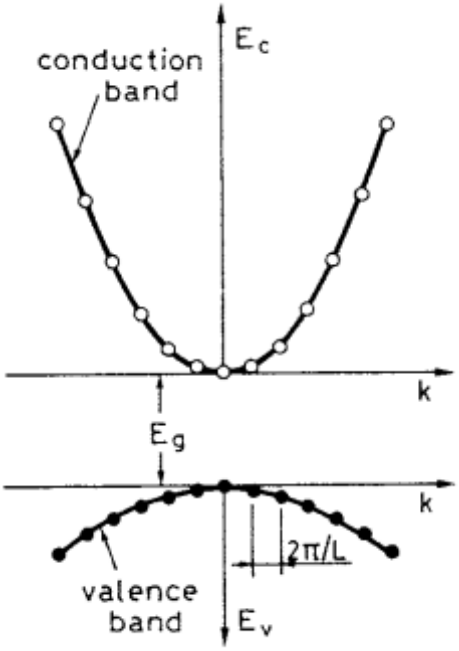


FIGURE 1.3: Two band model in the parabolic approximation [1]

The energies $E_c$ in the conduction band and $E_v$ in the valence band, measured from the bottom of the band upwards, can then be written as:

$$E_c = \frac{\hbar^2 k^2}{2m_c} \tag{1.1}$$

$$E_v = \frac{\hbar^2 k^2}{2m_v} \tag{1.2}$$

$k$, $m_c$ and $m_v$ are the wave number, the reduced mass of the electron at the bottom of the conduction band, given by $m_c = \hbar^2/[d^2E_c/dk^2]_{k=0}$ and the reduced mass of the electron at the top of the valence band, given by $m_v = \hbar^2/[d^2E_v/dk^2]_{k=0}$, respectively. It is easy to generalize this one dimensional case to a three dimensional one by defining the wave number as $k^2 = k_x^2 + k_y^2 + k_z^2$. One should also note that, for a finite sized medium (the simple situation being of a rectangular shaped medium with dimensions $L_x$, $L_y$ and $L_z$) we have to define the boundary conditions so that the total phase shift is an integer multiple of $2\pi$. This leads to:

$$k_i = \frac{2\pi n}{L_i} \tag{1.3}$$

where $i = x, y, z$ and $n$ is an integer. Now we can see the discrete nature of the levels within the bands as a result of the boundary condition. The black dots in figure 1.3 represent the energy states in the valence band and the open circles represent the energy states in the conduction band.

Supposing now that some electrons are raised to the conduction band by some pumping mechanism, the probability of an electron being on a given energy state $E$ within the valence or the conduction band is given by the Fermi-Dirac statistics:

$$f_c(E_c) = \frac{1}{1 + \exp \frac{E_c - E_{F_c}}{kT}} \tag{1.4}$$

$$f_v(E_v) = \frac{1}{1 + \exp \frac{E_{F_v} - E_v}{kT}} \tag{1.5}$$

$E_c$ and $E_v$ are the energy states in the bands, $E_{F_c}$ and $E_{F_v}$ are the Fermi levels of each band, $T$ is the temperature and $k$ is the Boltzmann's constant. Basically, the Fermi levels $E_{F_c}$ and $E_{F_v}$ at $T = 0$ K (as can be seen in figure 1.2 (B)) separate the regions where bellow them the states are fully occupied with electrons. This happens because the electrons relax to the lower energy levels within the band (with a typical relaxation time $\tau = 1$ ps). Spontaneous emission occurs when an electron drops from the conduction band to the valence band, recombining with a hole. This is called the recombination-radiation process and is the physical phenomena behind the light emitting diodes (LED).

Stimulated emission of radiation in a semiconductor can occur if the following condition is met:

$$E_g \leq h\nu \leq E_{F_c} - E_{F_v} \tag{1.6}$$

$E_{F_c}$ and $E_{F_v}$ depend on the intensity of the pumping radiation which means it also depends on the number $N$ of electrons raised to the conduction band, therefore it is more accurate to write $E_{F_c}$ and $E_{F_v}$ as functions of $N$, $E_{F_c}(N)$ and $E_{F_v}(N)$. Transparency of the medium is reached when there is gain exceeding losses, this being translated by the following condition:

$$E_g = E_{F_c} - E_{F_v} \tag{1.7}$$

### 1.1.1 Heterojunction Lasers

As previously said, it was only after the discovery of the heterojunction that we have been able to operate semiconductor lasers at room temperature. The homojunction has very high threshold current densities resulting in a high threshold pump power (the value at

which the laser starts amplifying the light) and cannot be operated in cw nor at room temperature. Laser performance can be optimized by reducing the threshold current density, as can be understood in the following discussion.

The unity round-trip condition is:

$$R_1 R_2 e^{2(\Gamma G_{th} - \alpha_{abs})L} = 1 \tag{1.8}$$

$G_{th}$ is the threshold gain $R_1$ and $R_2$ are the reflectivities of the active region's facets, $\Gamma$ is the confinement factor (the overlap between the lasing mode and the active region cross section), $L$ is the laser's length and $\alpha_{abs}$ the optical losses. Solving for the threshold gain:

$$G_{th} = \frac{1}{\Gamma}\left(\alpha_{abs} - \frac{\log(R_1 R_2)}{2L}\right) \tag{1.9}$$

For a bulk material the gain can be approximated as follows:

$$G = A_g(N - N_g) \tag{1.10}$$

Solving for N we get $N = \frac{G}{A_g} + N_g$. $A_g$ is the gain coefficient and $N_g$ is the carrier density needed to reach transparency. Another important approximation in this discussion is the injected carrier density, $N$, given as follows:

$$N = \frac{J\eta}{e\gamma_{eff}d} \tag{1.11}$$

$J$ is the injection current density, $\eta$ is the quantum efficiency, $e$ is the elementary charge, $\gamma_{eff}$ is the effective carrier recombination rate and $d$ is the active region's thickness.

We can now combine all of this quantities to derive an expression for the threshold current density, $J$, given as follows:

$$J_{th} = \frac{e\gamma_{eff}d}{\eta}\left\{N_g + \frac{1}{A_g\Gamma}\left[\alpha_{abs} - \frac{1}{2L}\log(R_1 R_2)\right]\right\} \tag{1.12}$$

Now, as we can see, the threshold current density depends heavily on the thickness of the active region - higher thickness means higher threshold current density - and this is where the heterojunction comes: we can block the current flow with a layer of a material with a higher band-gap energy than the active region. A heterojunction with just one blocking layer is called a single-heterojunction and one that has two blocking layers is called a double-heterojunction. A double-heterostructure where the active medium is GaAs is represented in figure 1.4.

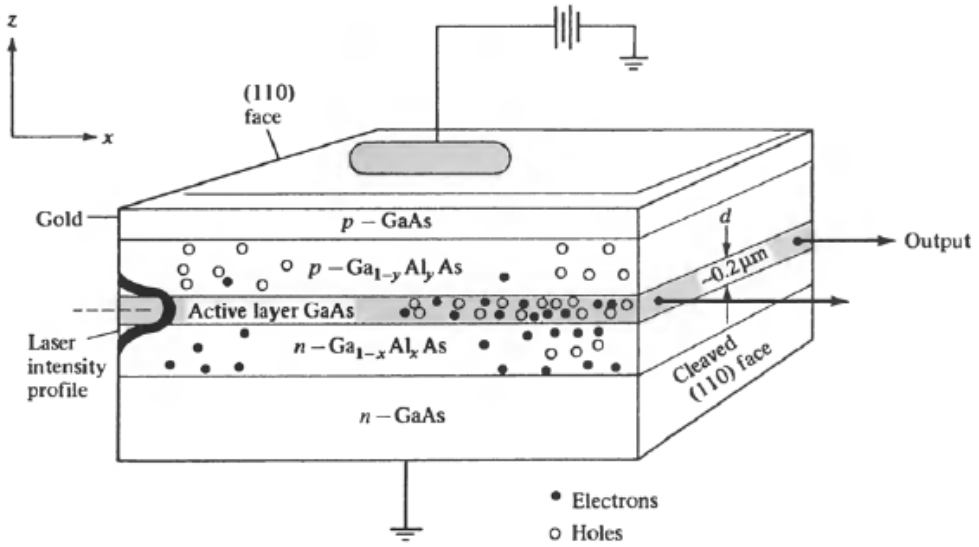


FIGURE 1.4: Double-Heterostructure [4]

To further visualize the properties of this structures both the index profile, the transverse beam profile and the band structure of a typical double-heterostructure are represented in figure 1.5. The reduction of the threshold current density is due to, primarily, three reasons: the two blocking layers, i.e. the $p$ and $n$ sides, as we can see in figure 1.5, have a lower index of refraction than the active medium which makes this structure to act like a waveguide. This results in the beam being more confined to the active medium which is where the gain exists; as we can see in figure 1.5, $E_{g_1}$ is smaller than $E_{g_2}$ which creates a blocking barrier in the two sides of the junction confining both electrons and holes to the active medium; the beam ($v = E_{g_1}/h$) is less absorbed in the cladding layers ($p$ and $n$ sides of the junction) than in the active medium.

Another important aspect that has to be considered when producing double heterostructures is the lattice period of the active medium: it has to be within 0.1% of the cladding layers. Figure 1.6 represents the lattice constant versus the wavelength corresponding to the energy band-gap.

The typical behaviour of the current as a function of the voltage in a laser diode is represented in figure 1.7:

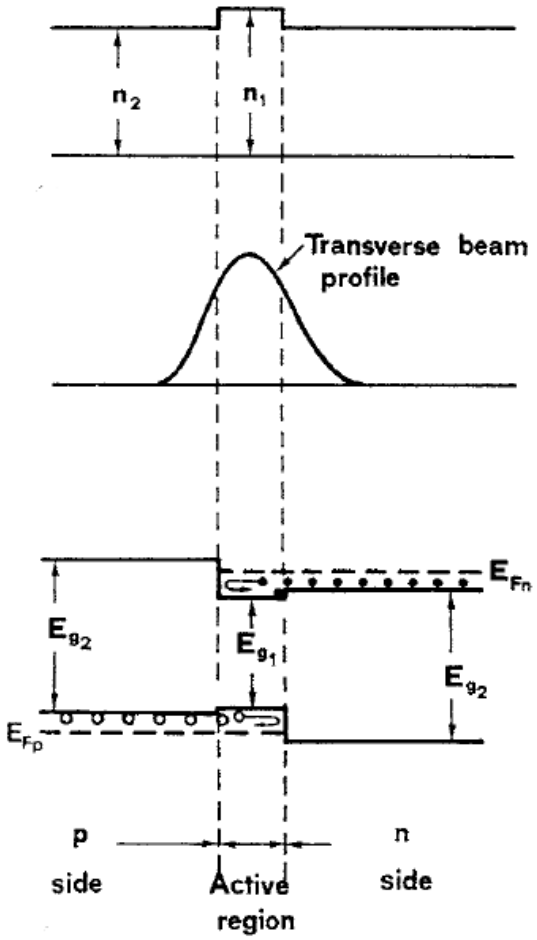


FIGURE 1.5: Index profile, transverse beam profile and band-structure of a typical double-heterostructure [1]

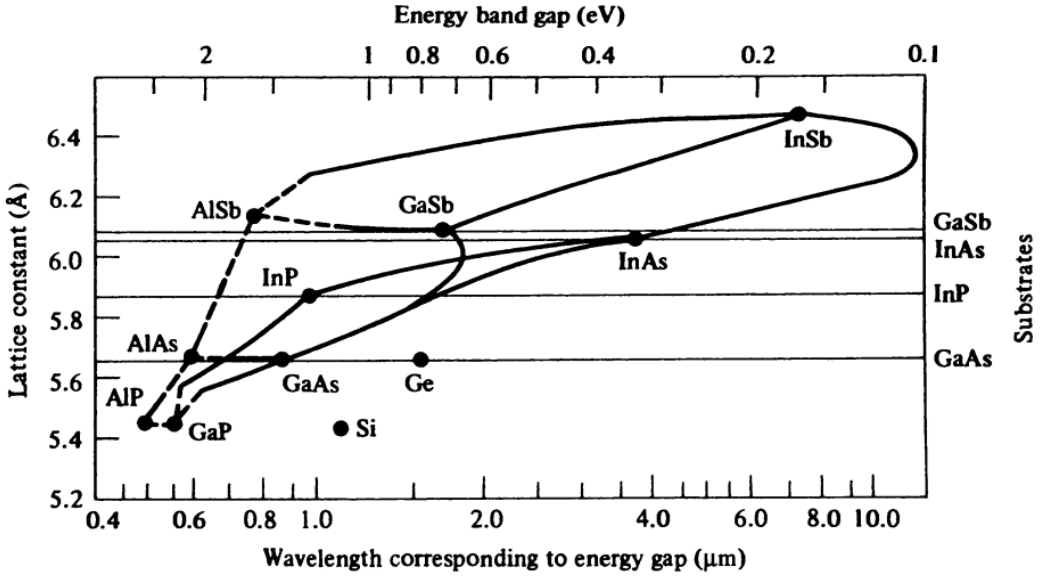


FIGURE 1.6: Lattice constant vs wavelength of the band-gap [4]

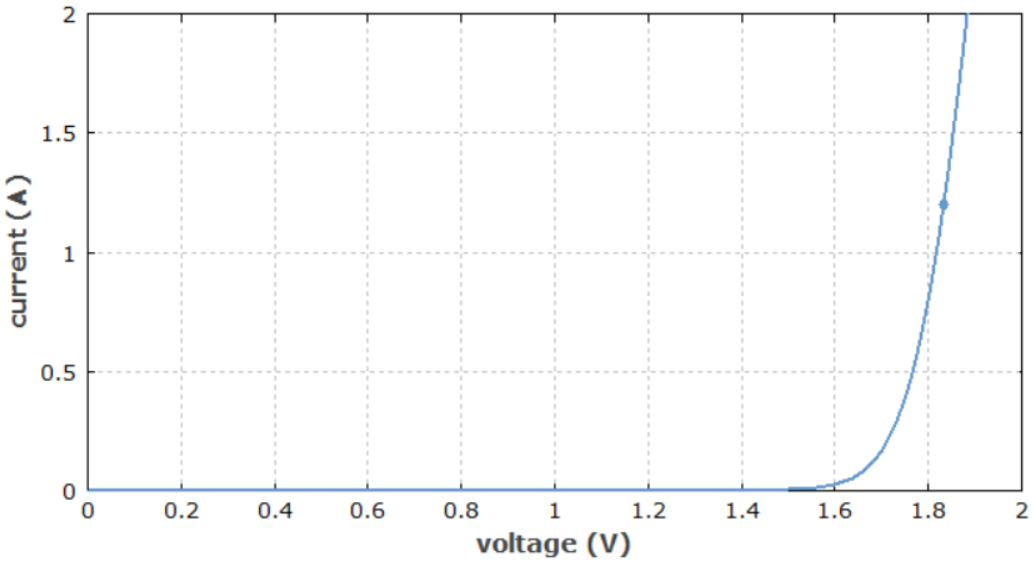


FIGURE 1.7: Current vs voltage curve of a laser diode [5]

## 1.2 Gaussian Beams

In this section we will explore the properties of a special solution of the wave equation: the Gaussian solution. We start by writing down the wave equation as follows [1]:

$$(\nabla^2 + k^2)\tilde{E}(x,y,z) = 0 \tag{1.13}$$

We can write the general solution for equation 1.13 within the paraxial wave approximation (small angles) in the form:

$$\tilde{E}(x,y,z) = u(x,y,z)e^{-jkz} \tag{1.14}$$

The Huygens-Fresnel-Kirchoff integral in the Fresnel approximation is:

$$\tilde{E}(x,y,z) = \frac{j\exp(-jk\,(z-z_1))}{\lambda\,(z-z_1)} \iint \tilde{E}\,(x_1,y_1,z_1) \exp\left\{ -jk\left[\frac{(x-x_1)^2+(y-y_1)^2}{2\,(z-z_1)}\right]\right\} dx_1 dy_1 \tag{1.15}$$

Substituting equation 1.14 into equation 1.15 one gets:

$$u(x,y,z) = \frac{j}{\lambda L}\iint_s u\,(x_1,y_1,z_1) \exp\left\{ -jk\left[\frac{(x-x_1)^2+(y-y_1)^2}{2L}\right]\right\} dx_1 dy_1 \tag{1.16}$$

Where we have $L = z - z_1$. $(x_1, y_1, z_1)$ and $(x, y, z)$ are the coordinates of the point $P_1$ and $P$, respectively. $P$ is the point $P_1$ after propagating by a distance $r$, as shown in figure 1.8:

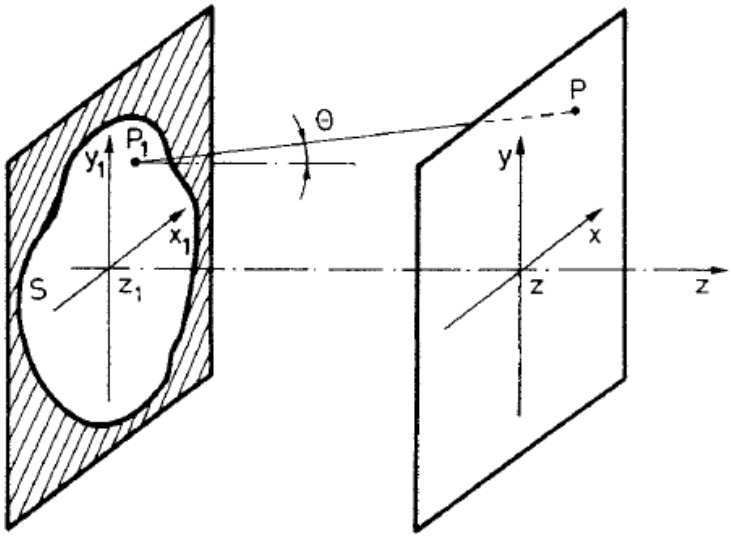


FIGURE 1.8: Field calculation after a distance $r$ [1]

Now let's consider the situation where this beam, still in the paraxial approximation, goes through a general optical system described by the *ABCD* matrix system where $u(x_1, y_1, z_1)$ is the field before entering the optical system and $u(x, y, z)$ is the field after the optical system, as shown in figure 1.9. One should note that this description works under the assumption that no field-limiting apertures are present in the optical system.

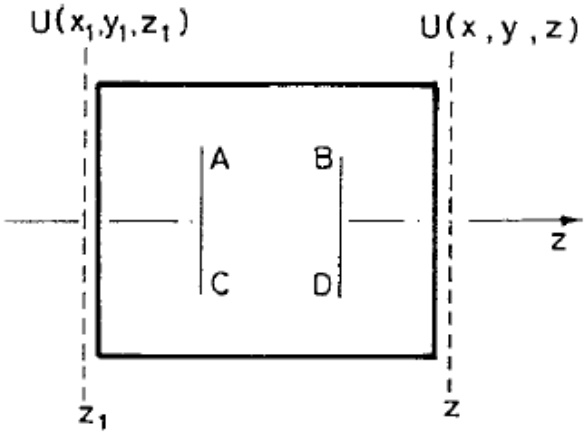


FIGURE 1.9: Field calculation after a distance $r$ through a general optical system described by the *ABCD* matrix [1]

Then, equation 1.16 becomes:

$$u(x,y,z) = \frac{1}{B\lambda}\iint_s u\left(x_1,y_1,z_1\right)\exp\left\{-jk\left[\frac{A\left(x_1^2+y_1^2\right)+D\left(x^2+y^2\right)-2x_1x-2yy_1}{2B}\right]\right\}dx_1dy_1 \tag{1.17}$$

We can see that for $A = D = 1$ and $B = L$ the beam goes through free space. The solution for equation 1.17 is:

$$u(x,y,z) = \frac{1}{A+\left(B/q_1\right)}\exp\left(-jk\frac{x^2+y^2}{2q}\right) \tag{1.18}$$

Where $q$ is the complex beam parameter after the optical system and $q_1$ is the complex beam parameter before the optical system. $q$ and $q_1$ are related to each other by equation 1.19:

$$q = \frac{Aq_1+B}{Cq_1+D} \tag{1.19}$$

After combining equations 1.18 and 1.14 we can arrive at the following equation for the inverse of the complex beam parameter:

$$\frac{1}{q} = \frac{1}{R} - j\frac{\lambda}{\pi w^2} \tag{1.20}$$

Equation 1.20 is of extreme importance for calculations of Gaussian beam propagation as it relates the complex beam parameter to the radius of curvature of the wavefront, $R$, and to the beam waist, $w$.

The following discussion will be centered in the free space propagation of laser beams and through optical media (namely thin lenses) as this will be of extreme importance for the experimental part of this work.

Let's consider a laser beam propagating through the positive direction of the z axis and set $z = 0$ to the position of the beam's waist. The complex beam parameter $q$ after propagating a distance z will be:

$$q = q_1 + z \tag{1.21}$$

And the inverse of $q_1$ will be:

$$\frac{1}{q_1} = -j\frac{\lambda}{\pi w_0^2} \tag{1.22}$$

$w_0$ is the spot size of the beam. From equations 1.21 and 1.22 we can deduce the following and very useful equations:

$$w^2(z) = w_0^2 \left[1 + \left(\frac{\lambda z}{\pi w_0^2}\right)^2\right] \tag{1.23}$$

$$R(z) = z \left[1 + \left(\frac{\pi w_0^2}{\lambda z}\right)^2\right] \tag{1.24}$$

$$\phi = \arctan\left(\frac{\lambda z}{\pi w_0^2}\right) \tag{1.25}$$

There are some quantities which characterize the laser beam that are very important to know when we are working with lasers and communicating with other people. Many of them are related to the profile of the beam near the focus (the waist location) and away from the focus. Figure 1.10 and 1.11 illustrate very well this characteristics:

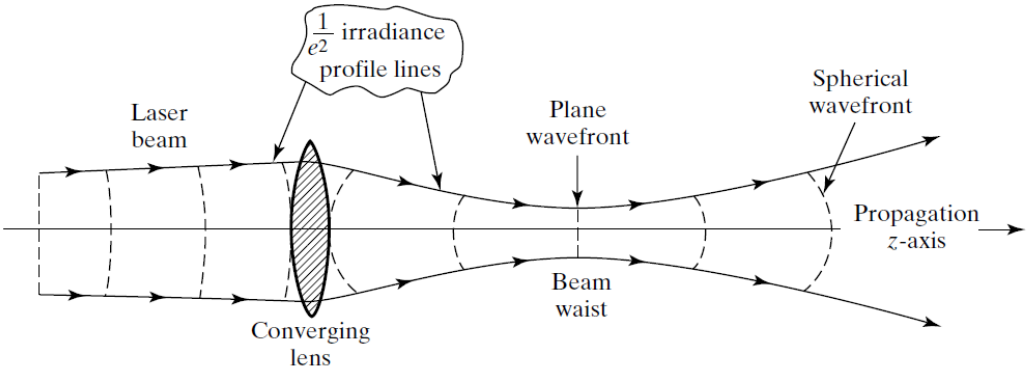


FIGURE 1.10: Waist after the beam goes through a thin lens. The incoming beam is collimated so that the wavefronts are planar and, after the lens, curved [6]

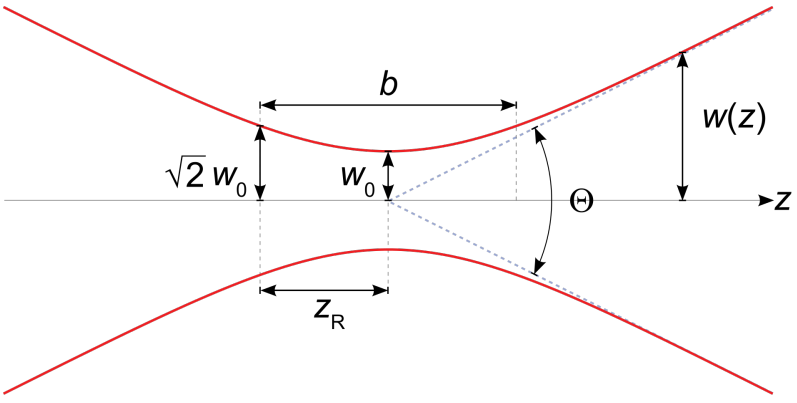


FIGURE 1.11: Some important quantities in the beam's waist [7]

In figure 1.10 one should note that the lines that trace the beam profile are calculated at the points where the field is $\frac{1}{e^2}$ of its maximum irradiance. This concept will be important for the $M^2$ measurements. Another important quantity is the *Rayleigh range* which is the distance along the propagation direction of a beam from the waist to the place where the area of the cross section is doubled [8], defined by the following equation:

$$z_R = \pi \frac{w_0^2}{\lambda} \tag{1.26}$$

The angle $\Theta$ is defined as $\Theta = 2\theta$ where $\theta$ is:

$$\theta = \frac{\lambda}{\pi w_0} \tag{1.27}$$

Finally, with simple linear algebra and help from the *ABCD* matrix system we can calculate the position of the waist after the beam passes through a thin lens and its spot size:

$$z_m = f / \left[1 + \left(f / z_{R_1}\right)^2\right] \tag{1.28}$$

$$w_{02} = \lambda f / \pi w_{01} \left[1 + \left(f / z_{R_1}\right)^2\right]^{1/2} \tag{1.29}$$

$z_m$ is the waist's location relative to the lens, $w_{01}$ is the beam's spot-size at the lens, $z_{R1}$ is the Rayleigh range at the lens and $w_{02}$ is the beam's spot-size at the waist. For $z_{R1} >> f$ equations 1.28 and 1.29 become:

$$z_m = f \tag{1.30}$$

$$w_{02} = \lambda f / \pi w_{01} \tag{1.31}$$

## 1.3 Diode Lasers as Pump Sources

Since the first demonstration of a Ti:Sapphire laser working in cw directly pumped by a 1W, 452nm Gallium Nitride (GaN) laser diode by Roth *et. al.* [9] that this technology is being more and more explored. What made this possible was the development in the 90's of blue diode lasers based on indium gallium nitride [10] which now opens the market for Ti:Sapphire lasers directly pumped by high power blue laser diodes. Although the beam quality of laser diodes is not great, mode-locking in the femtosecond regime has also been achieved using these lasers as demonstrated by Roth *et. al.* [11] by using a single 1W GaN-based diode laser operating at 452 nm and generating pulses as short as

114 fs. Recently, Han Liu *et. al.* [12] demonstrated mode-locking in the sub-10 femtosecond regime using a single 3.5W, 455 nm diode laser directly pumping a ti:sapphire laser which shows the possibility for these lasers to be used in medical applications such as eye surgery, in microscopy and in metrology.

Ti:sapphire is the active medium used for achieving the shortest optical pulses and the largest bandwidths directly from a laser. This is because the crystal has a very large emission bandwidth as can be seen in the picture 1.12:

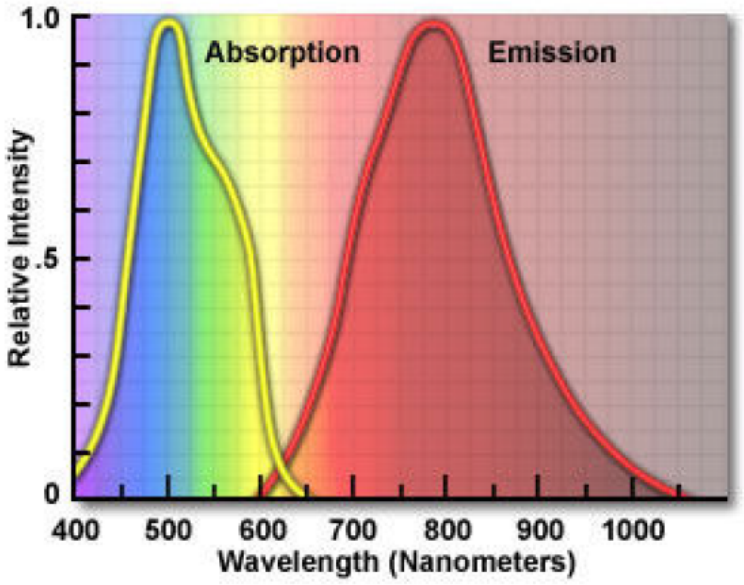


FIGURE 1.12: Ti:sapphire's emission and absorption spectrum [13]

There are essentially four types of laser diodes as pump sources: single-stripe, diode-array, diode-bar and stacked-bars. Single-stripe diode lasers have a broad shaped stripe emitting area, with typical dimensions of 1µm×100µm, as we can see in figure 1.13:

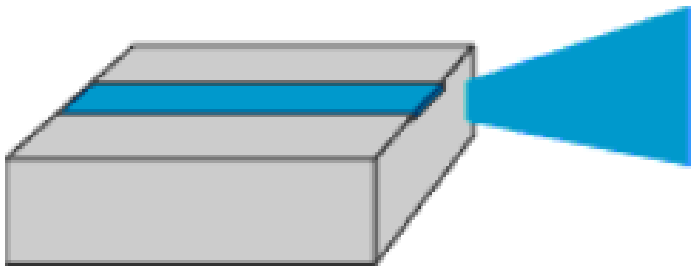

FIGURE 1.13: Single-Stripe laser diode [14].

Due to the asymmetry of the emitter the beam has distinct properties on both directions. On the vertical direction (typical dimensions around 1µm) the height is small enough to produce a near diffraction-limited beam and accommodate just one mode

which leads to the $M^2$ being approximately 1. On the other side, because the aperture size is so small the beam divergence on this direction is very high. Due to this fast divergence this is called the fast axis. On the horizontal direction (typical dimensions around 50, 100, 200µm or even larger) the stripe width is large enough to accommodate many spatial modes and the divergence of the beam is much smaller. Because the beam divergence is slower this is called the slow axis.

To obtain more optical power one can use an array of diode laser-stripes fabricated on the same substrate. A scheme of a typical diode-array is shown in figure 1.14:

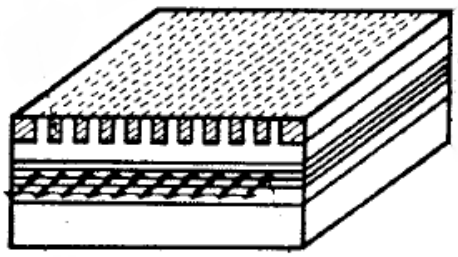

FIGURE 1.14: Typical diode-array [1]

In order to obtain even more optical power one can serially repeat the array described above, each typically having between 20 to 50 stripes. Important parameters for constructing these systems are the spacing between each array and the number of stripes each array has. A scheme of a typical diode-bar is shown in figure 1.15:

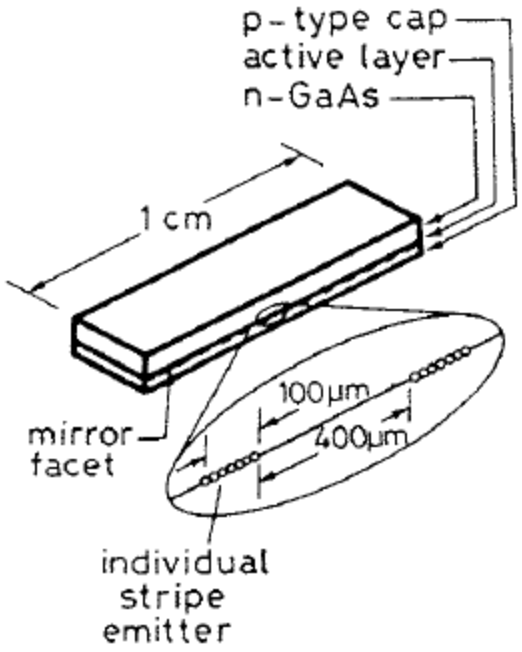


FIGURE 1.15: Typical diode bar [1]

One can extend to the case of a stack of bars to form a two dimensional structure for obtaining even more optical power. A scheme of a typical stack of bars is shown in figure 1.16:

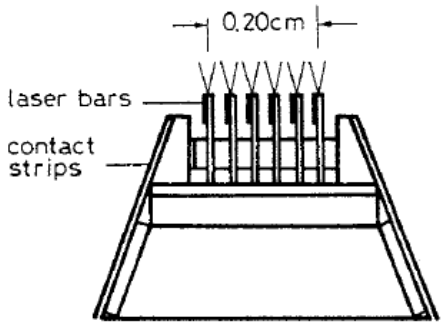


FIGURE 1.16: Stacked-bars [1]

### 1.3.1 Longitudinal Pumping

Longitudinal pumping (or end pumping) is a technique of pumping the active medium where the pump light is along the same direction as the amplified light. The most common configurations of this type of pumping are shown in figure 1.17: The three configurations are: configuration (a) - the single-ended pumping in a simple plane-concave

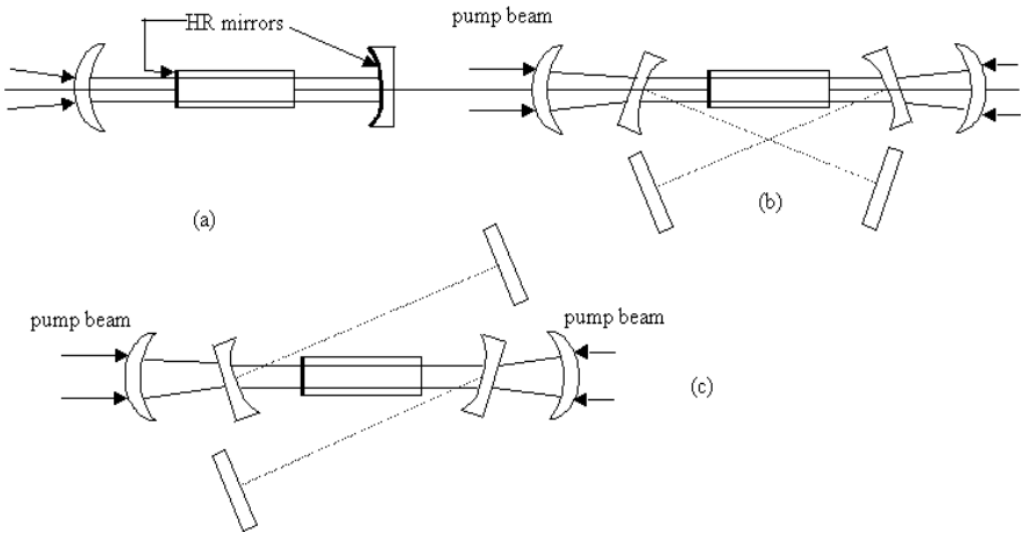


FIGURE 1.17: Longitudinal diode laser pumping [15]

resonator; configuration (b) - the double-ended pumping for an X-shaped linear cavity; and configuration (c) - the double-ended pumping for a z-shaped folded linear cavity.

Due to the strong asymmetry of the output beam from the laser diode covered in the beginning of section 1.3, careful modelling of the beam shape has to be performed in order for it to be focused on the active medium.

Let's consider the case of the single stripe laser diode represented in figure 1.13. In a laser diode the fast axis and the slow axis usually have different divergence angles and, because of that, if we put a lens in front of the laser diode the beam will focus in two different locations (one after the other). We call this astigmatism and it is a problem that has to be solved in order to focus the beam on the Ti:Sapphire crystal. Another well know characteristic of a laser diode is its poor beam quality. This is quantified by the $M^2$ *factor* which measures how much can a beam be focused relative to a diffraction-limited one. The half-angle beam divergence is given by equation 1.32:

$$\theta = M^2 \frac{\lambda}{\pi w_0} \tag{1.32}$$

where $M^2$ is the $M^2$ *factor*, $\lambda$ is the wavelength and $w_0$ is the beam's spot radius. A watchful reader will recognize this equation as being similar to equation 1.27. In truth, equation 1.32 is just an adaptation of equation 1.27 for a non diffraction-limited beam which has an $M^2$ *factor* of 1 and is a *Gaussian* beam. The output beam of a laser diode usually has lower $M^2$ *factor* for the fast axis and a bigger one for the slow axis. One should note that it is impossible to have values of the $M^2$ *factor* smaller than 1. Knowing the $M^2$ *factor* for both

the fast and the slow axis is of extreme importance in order for us to know how much we can focus the beam and how can we improve other aspects of the beam in order to have the smallest spot size possible in the crystal. After knowing both the divergences and the $M^2$ *factors* of the fast and slow axis it is common to use a combination of a spherical lens and a pair of cylindrical lenses (usually in telescopic configuration) to shape the beam.

### 1.3.2 Brief Review of Diode-Pumped Laser Systems

When designing the pumping system for the oscillator several technical characteristics have to be taken into consideration since we want to have a mode-locked laser operating in the femtosecond regime. The optical bandwidth, average output power, time duration of the pulses and pulse power are key aspects that we took into consideration when preparing the setup for the laser. We looked in the literature and compared four ti:sapphire laser systems directly pumped by laser diodes which had the best results to date.

Table 1.1 shows the comparison between Laser 1 [12], Laser 2 [16], Laser 3 [17] and Laser 4 [18]:

| | **Laser 1** | **Laser 2** | **Laser 3** | **Laser 4** |
|---|---|---|---|---|
| **Temporal Width (fs)** | 8.1 | 13.5 | 15 | 48 |
| **Average Optical Power (mW)** | 27 | 145 | 170 | 360 |
| **Bandwidth (nm)** | >146 | >80 | 74.6 | 14.4 |
| **Repetition Rate (MHz)** | 120.6 | 78 | 87 | 117 |
| **Energy per Pulse (nJ)** | 0.224 | 1.85 | 1.95 | 3.08 |
| **Temporal Diagnostic** | IAC | FROG | IAC | IAC |
| **Pump** | One 3.5 W (455 nm) LD | One 3.1 W (465 nm) LD | One 4.4 W (461 nm) LD | Four 1 W (478 and 520 nm) LDs |

TABLE 1.1: Comparison between four of the most state of the art ti:sapphire lasers directly pumped by laser diodes.

Based on this research we concluded that our best option would be one high power laser diode with a peak emission wavelength around the peak of the absorption spectrum

of the Ti:Sapphire. Considering the market availability at that moment we chose a blue (470 nm) laser diode (more about it in section 2.2).

# Chapter 2

# Blue Laser Diode

Laser diodes are devices extremely sensitive to temperature, electrostatic discharge, sudden variations of the electric potential and stress. Just by touching the laser diode without specific ESD (*Electrostatic discharge*) equipment, letting it fall off the working table or having the soldering iron set up to a very high temperature we can permanently damage the device. Because of that careful handling and appropriate working procedures have to be taken so that we don't damage or destroy it.

In this chapter we will cover all the procedures that have been taken within the preparation and characterization of the chosen laser diode, some of the basic functionalities of both the laser diode and its driver and all the measurements that were performed.

## 2.1 Requirements Analysis

Since we wanted a laser diode in a specific range of wavelengths and with enough optical power capable of pumping a Ti:Sapphire oscillator we started by searching on the literature for the type of laser diodes were the most used. We knew that we needed a diode with its peak wavelength near the Ti:Sapphire absorption peak (500 nm figure 1.12) and with an optical power of at least 2W. We found out that the most used ones were either blue or green (or a combination of both) in the region of $\approx [510, 520]$ nm ([19], [20], [21], [22], [23], [24]) and $\approx [450, 480]$ nm ([19], [16], [17], [12], [23]). We also needed a driver that could provide a stable current to the laser diode and protect it from abrupt transients.

## 2.2 The Laser diode

We chose the *Nichia NUBM07E 465nm* laser diode which is rated to 3.5A of maximum working current. The datasheet of the diode is shown in table 2.1:

FIGURE 2.1: *Nichia NUBM07E 465nm* laser diode

| Item | Condition | Symbol | Min | Typ. | Max | Unit |
|---|---|---|---|---|---|---|
| **Optical Output Power** | If = 2.3 A | Po | - | (2.9) | - | W |
| **Dominant Wavelength** | If = 2.3 A | $\lambda$d | 458 | 465 | 472 | nm |
| **Threshold Current** | CW | Ith | 300 | - | 550 | mA |
| **Slope Efiiciency** | CW | $\eta$ | - | (1.6) | - | W/A |
| **Operating Voltage** | If = 2.3 A | Vop | 3.7 | - | 4.9 | V |
| **Beam Divergence (Parallel)** | If = 2.3 A | $\theta_{\parallel}$ | 0.25 | (0.40) | 0.55 | deg |
| **Beam Divergence (Perpendicular)** | If = 2.3 A | $\theta_{\perp}$ | -0.8 | (0.1) | 0.8 | deg |

TABLE 2.1: Specifications of the *Nichia NUBM07E 465nm*.

As we can see from table 2.1 the diode is rated with a typical optical output power of 2.9W and a maximum working current of 3.5A (the full datasheet can be found on Appendix A). With it came the driver and dedicated housing, heat sink and fan (*Yakoo dc brushless fan 12v, 0.1A*). The diode's driver is shown in figure 2.2.

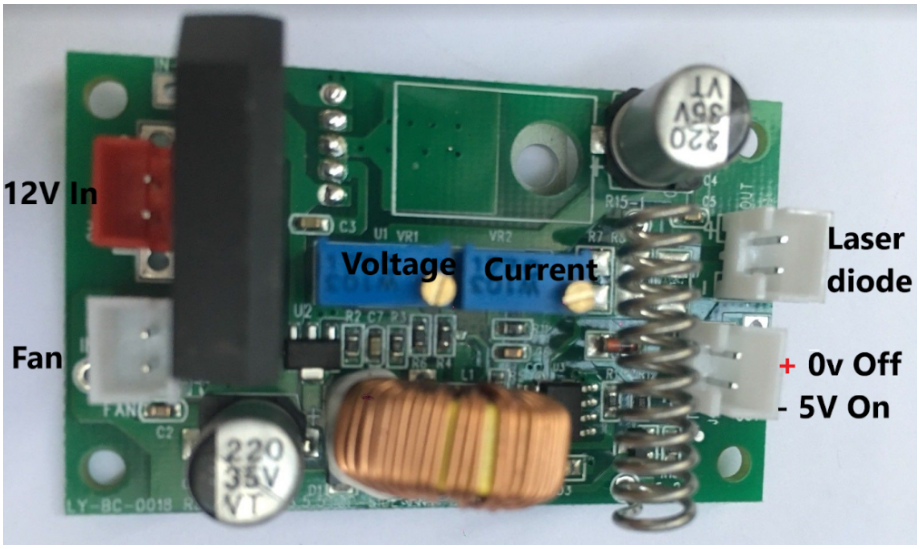


FIGURE 2.2: Laser diodes's driver (*ly-bc-0018 PCB*)

## 2.3 *ly-bc-0018 PCB* driver characterization

Firstly, we tested all the connections with a multimeter in order to find out if the circuit board was functional. The biggest concern in performing the characterization of the circuit board was whether or not it was capable of providing a stable current to the laser diode without abrupt transients. If it was not capable of doing such thing we would have to modify it. After verifying with a multimeter that all the connections were perfectly working we made simple measurements of all the outputs of the PCB, specifically, the 12V input, the fan, the laser diode input and the TTL. We used a *Tenma 72-10480 digital-control* DC power supply and the measurements are represented in the table 2.2:

From table 2.2, we see that the driver provides a constant voltage for both the laser diode and the TTL terminals and a variable voltage for both the fan and the input terminals which is precisely what we want: a stable voltage/current for the diode. The driver is factory set for working between 9 and 12 Volts so we decided to work with 12V which is the voltage that provides more power to the fan. It should be noted that this measurements were performed with the power supply limited to 1A and that the TTL was not used in this work.

| Power Supply (V) | Laser Diode (V) | Fan (V) | TTL (V) | Input (V) |
|---|---|---|---|---|
| 9 | 4.704 | 7.30 | 4.621 | 8.86 |
| 10 | 4.704 | 8.30 | 4.626 | 9.86 |
| 11 | 4.708 | 9.30 | 4.628 | 10.88 |
| 12 | 4.708 | 10.31 | 4.627 | 11.88 |

TABLE 2.2: Circuit board measurements for the power supply being limited to 9, 10, 11 and 12 Volts.

Further tests were made exploring the performance of the driver with one and two halogen lamps 2.3. This lamps were connected both in series and in parallel and the

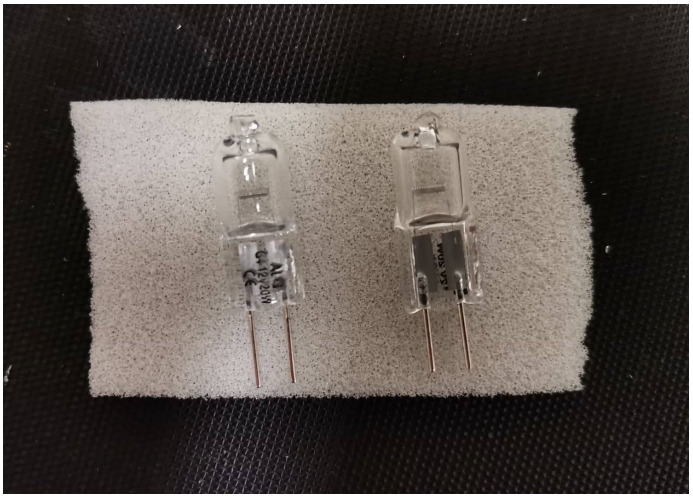

FIGURE 2.3: Two lamps rated for 20W and 12V.

results are shown below:

It should be noted once again that all this measurements were made with the power supply set for limiting the current to 1A.

By looking at the data from tables 2.3, 2.4 and 2.5 we can see once again the expected driver's behavior: a stable current for the lamps. When performing this measurements in the parallel setup (table 2.5) we also noticed that the blue potentiometers in the circuit board, 2.2, were limiting the current in the laser diode input to 1A since we could see that the lamps were not as bright as in the series configuration and the power supply could not provide more than 1A.

| Power Supply (V) | Lamp 1 (A) | Power Supply (A) |
|---|---|---|
| 9 | 0.86 | 0.625 |
| 10 | 0.86 | 0.560 |
| 11 | 0.86 | 0.507 |
| 12 | 0.86 | 0.467 |

TABLE 2.3: Measurements performed with just one halogen lamp.

| Power Supply (V) | Lamp 1 + Lamp 2 (A) | Power Supply (A) |
|---|---|---|
| 9 | 0.64 | 0.464 |
| 10 | 0.64 | 0.417 |
| 11 | 0.64 | 0.380 |
| 12 | 0.64 | 0.350 |

TABLE 2.4: Measurements performed with two lamps connected in series.

| Power Supply (V) | Power Supply (A) | Lamp 1 (A) | Lamp 2 (A) |
|---|---|---|---|
| 9 | 0.998 | 0.48 | 0.46 |
| 10 | 0.998 | 0.48 | 0.46 |
| 11 | 0.998 | 0.48 | 0.46 |
| 12 | 0.998 | 0.48 | 0.46 |

TABLE 2.5: Measurements performed with two lamps connected in parallel.

Still working with lamps we wanted to test the transient behavior (when turning on the power supply) before connecting the driver of the laser diode. For this we connected the oscilloscope, set the trigger level to single shot and adjusted its level to approximately half the voltage of when the lamp is turned on in order to freeze the transient. We also tweaked the temporal scale in order to successfully freeze the transient. The result for 12V is shown in figure 2.4:

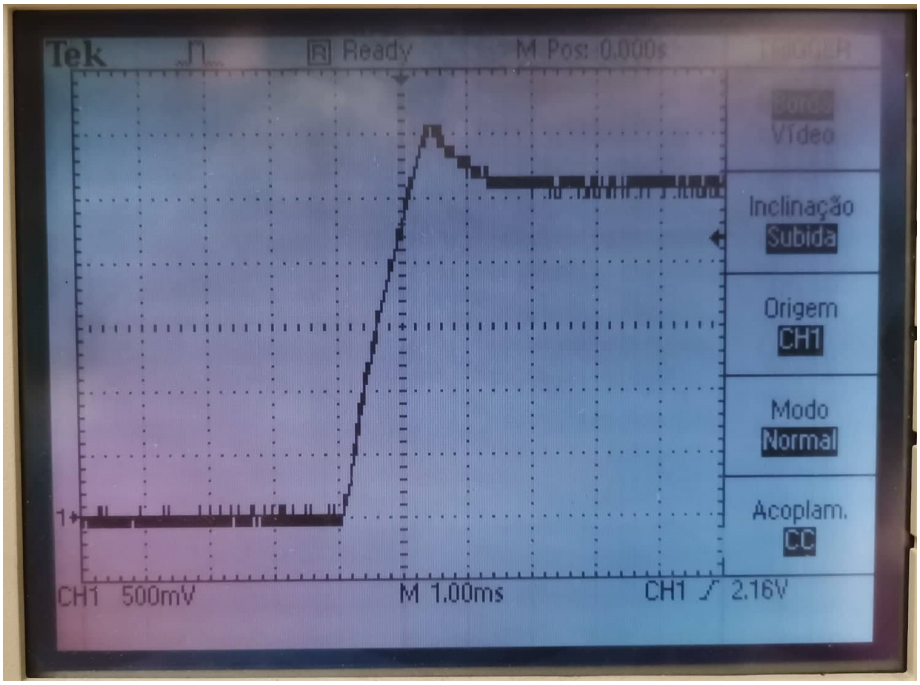


FIGURE 2.4: Halogen lamp transient. Power supply set up to 12V.

We can notice some degree of overshooting of around 0.5V. The transient duration is approximately 2.5ms which is a very slow transient for a laser diode [25]. Since we wanted a wall mount power supply to power up the laser we also measured the transient with one. The result is shown in figure 2.5.

With this experiments we were more confident to connect the laser diode to the driver and begin its characterization.

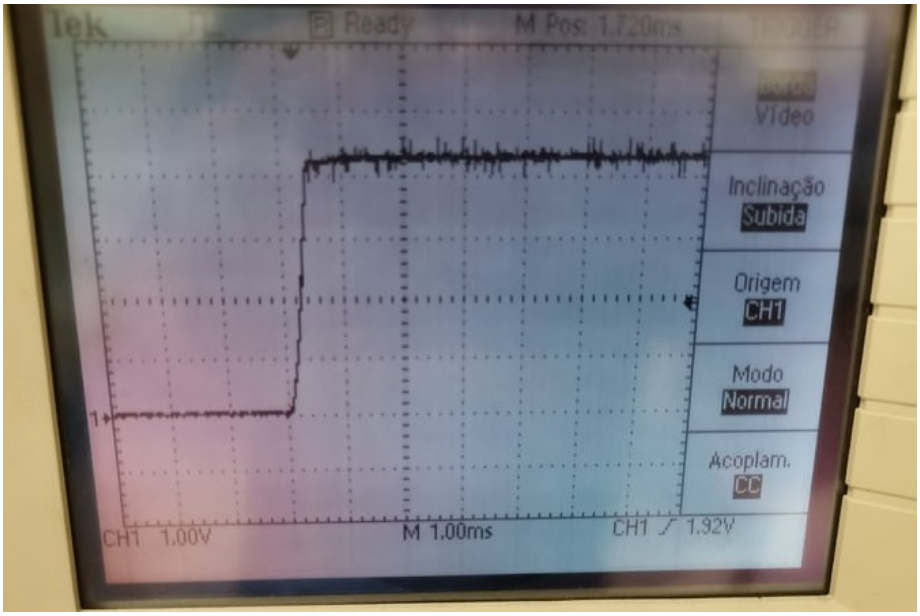


FIGURE 2.5: Halogen lamp transient. 12V wall mount power supply.

## 2.4 Safety procedures

One of the biggest concerns regarding the handling of laser diodes was already discussed in section 2.3 but this devices require a lot more attention than just making sure that the driver protects them from abrupt transients.

But before discussing some of the safety procedures that one has to take in order to safely handle laser diodes we should firstly discuss some of the habits we have to take when working with lasers so that we don't hurt ourselves. It is known that lasers can damage our eyes and even blind us. That is because our eyes were developed to focus visible light (380 to 700nm) in the retina (our light sensor). Equipment such as laser goggles, laser cards (to block the beam), signs, etc, were used to prevent damage in our eyes.

### 2.4.1 Temperature control

In a lot of applications, a good control of temperature improves the performance of optoelectronic devices, such as laser diodes. This applies even to detectors such as power meters, that will be important later on this work. Also, the operating characteristics of laser diodes vary according to their working temperature which means that a proper heat dissipation has to be done when we want to operate with this kind of devices [26]. What happens is that, if the heat dissipation is not sufficient, the laser diode will reach a peak optical power and decrease until it goes to zero.

The most used dissipating systems are the thermoelectric devices (*Peltier*) and heat sinks (anything that is in contact with the laser diode that has a cooling effect, such as metal, thermal paste and even air). We used heat sinks in order to provide great heat dissipation of the laser diode, more specifically a cylindrical-shaped piece of aluminium which served as housing for the laser diode, a parallelepiped-shaped piece of aluminium which is where the housing is and stays in close contact with a breadboard where we screwed in this system. Both the cylindrical and the parallelepiped-shaped pieces of aluminium are represented in figure 2.6.

FIGURE 2.6: Cylindrical and parallelepiped-shaped pieces of aluminium that serve as heat sink for the laser diode.

We also used another breadboard as a heat sink for the driver since we noticed that some electrical components were heating too much. We used another breadboard in order for the laser and the driver to be isolated from each other and prevent conduction of electricity between them. This setup is shown in figure 2.7 (schematic in figure 2.8).

Other than heat sinks we also used thermal paste for improving the contact between the laser diode and its housing, improving the contact between the housing and the parallelepiped-shaped heat sink and improving the contact between the latter and the breadboard.

Finally, and one of the most meticulous tasks in this chapter was soldering the wires to the laser diode's terminals. In order to avoid serious damage we soldered one terminal at a time with the iron at 350ºC and made sure that we would not be with the tip of the iron in contact with the terminal for more than three seconds. We also waited until the laser diode had cooled down before starting to solder the other terminal.

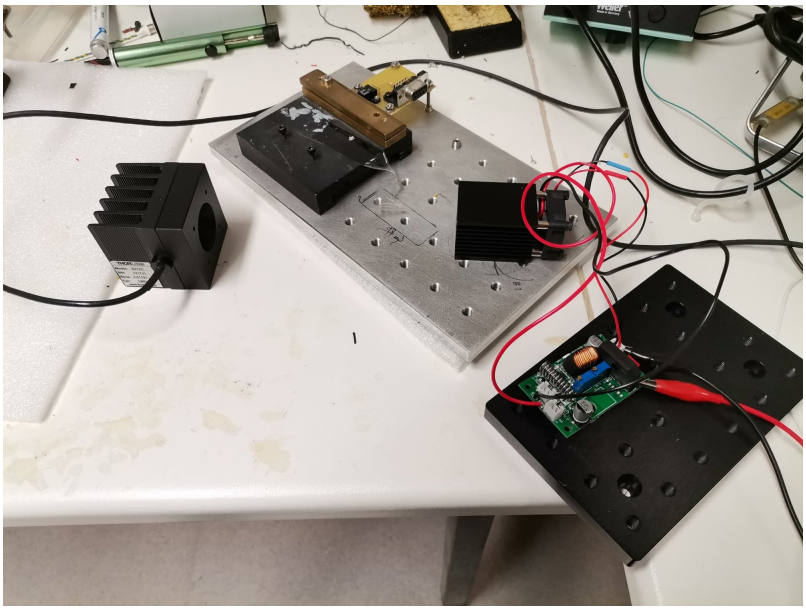

FIGURE 2.7: Experimental setup for the characterization of the laser diode.

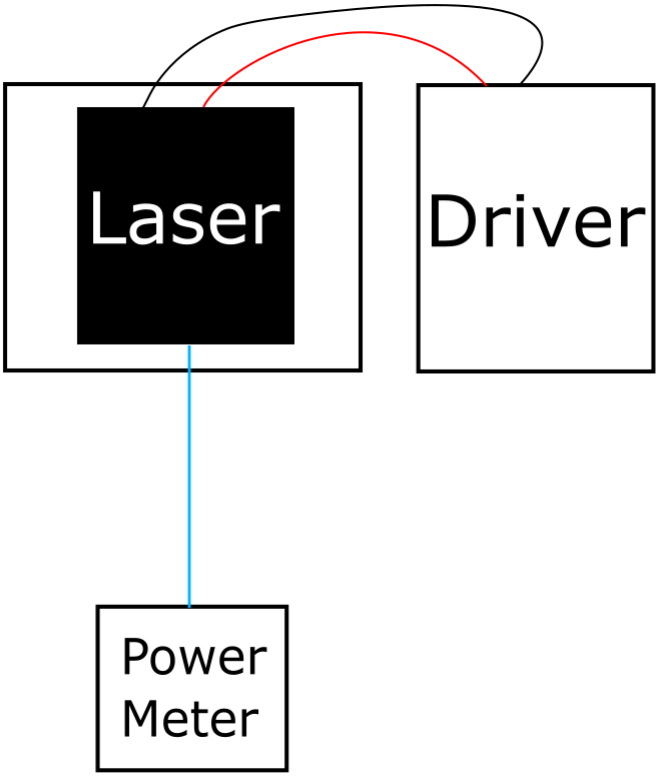


FIGURE 2.8: Schematic of the setup for the characterization of the laser diode. Top view.

After we arranged the setup represented in figure 2.7 we noticed that the laser was still not stabilized, meaning that it still would reach a peak optical power and than decrease from that. To solve this problem we put a 10W, 12V DC *Sunon MEC0381V1-000U-G99 120x120x38mm* fan and rearranged the setup in order for the fan to cool both the driver and the laser diode. With this new setup we finally stabilized the laser with a constant optical power. We then set the blue potentiometer relative to the current for an optical output power of 3.3W. This setup is represented in figure 2.9 and in figures 2.10 (A) and (B) (schematic shown in figure).

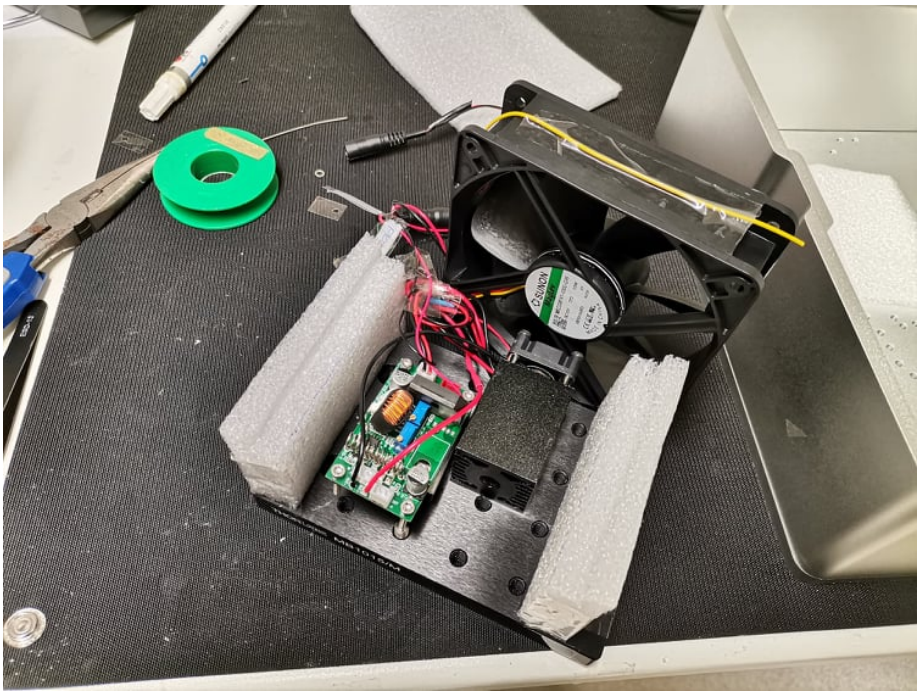

FIGURE 2.9: Final setup.

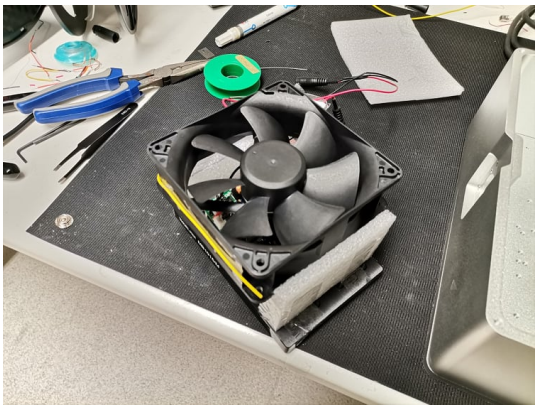

(A) Top view.

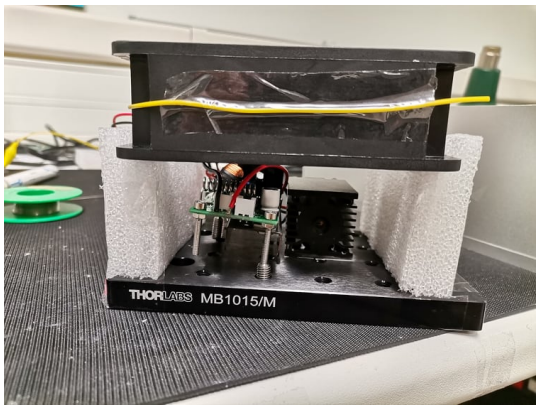


(B) Front view.

FIGURE 2.10: Final setup in top and front view.

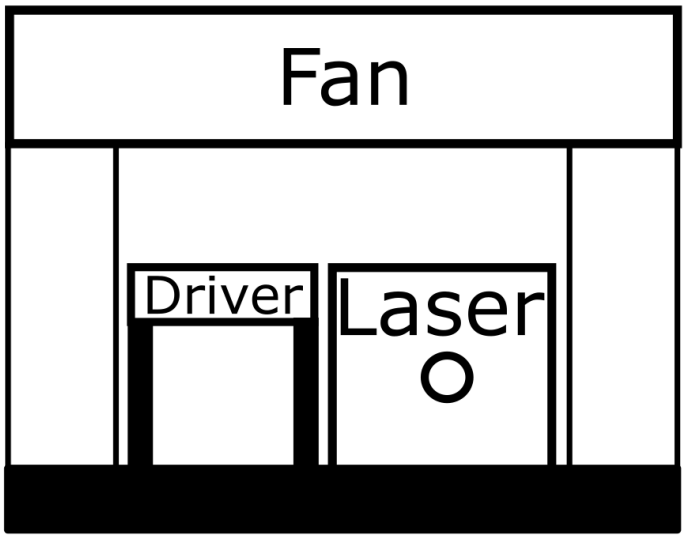


FIGURE 2.11: Schematic of the final setup. Front view.

### 2.4.2 ESD safety

Laser diodes are very sensitive to electrostatic discharges which makes ESD (Electrostatic Discharge) procedures essential for handling this devices and this basically means that the workplace has to be grounded [27]. We used a dedicated ESD mat above the working table and wrist bands so that we could safely handle the laser diode and made sure that all the used equipment was above the mat. The setup is represented in figure 2.12:

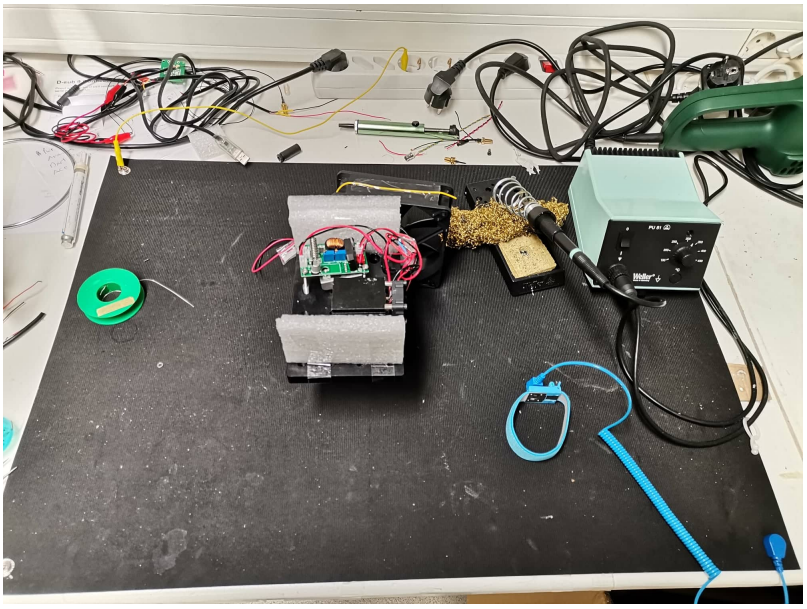

FIGURE 2.12: ESD setup used throughout the laser diode's assembly and characterization.

## 2.5 Laser Diode Characterization

The very first thing we did with the setup represented in figure 2.7 was measuring the transient behaviour. We obtained the following result:

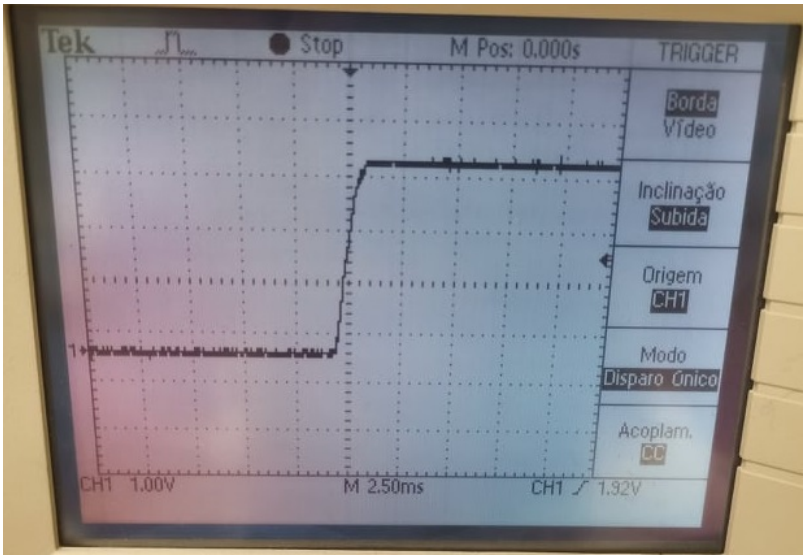


FIGURE 2.13: Transient of the driver's output connected to the laser diode.

We can notice a very smooth transient with a duration of approximately 1.25ms. Since we don't have any overshooting and comparing to the transients that William G. Olsen *et. al.* [25] obtained in their work which were in the order of the microsecond we could proceed our work with confidence. After this we wanted to measure the current that was passing through the diode so that we could monitor it in a controlled way. The reader should note that, as shown in the diode's datasheet in appendix A, the maximum current is 3.5A. We had to work with 2.57A since this was the maximum current in which we had a stable output optical power. We could achieve a higher optical power (and so a higher working current) through active cooling, but we did not have the necessary equipment for doing it. For this we had to cut the wire that was soldered to the diode's positive terminal and solder both the cut ends to two connectors so that we could plug into the multimeter. The setup is represented in figure 2.14 (schematic in figure 2.15).

As already discussed in subsection 2.4.1 the driver and diode's temperature stabilization, and consequentially optical power, was a big challenge to achieve. In order to properly characterize these two parameters we used a *Thorlabs PM100A* power meter and a *TEMPerHUM USB* temperature and humidity sensor and for each sensor we wrote a *Python* script to acquire simultaneously the data through a *Raspberry Pi*.

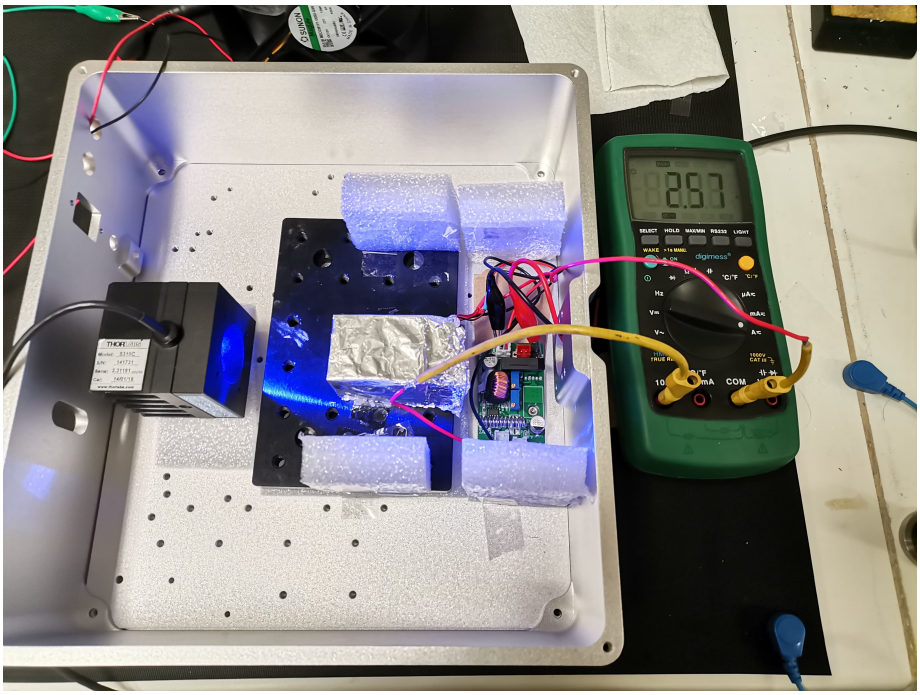

FIGURE 2.14: Setup for the measurement of the current that was passing through the laser diode.

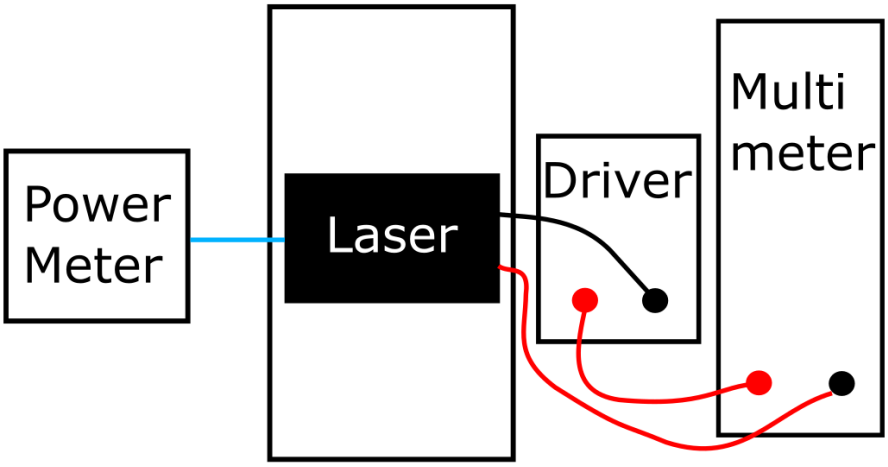


FIGURE 2.15: Schematic of the Setup for the measurement of the current that was passing through the laser diode. Top view.

The power meter code is based on a *Python* library developed by *Thorlabs* called *ThorlabsPM100* [28] which in combination with *PyVisa* [29] can read the sensor's data. *PyVisa* simply lets the user to connect to the instrument and *ThorlabsPM100* reads the data (the script that we used is represented in appendix B). Then we just added a *while* loop for the code to be constantly reading the data.

For the temperature and humidity sensor we used a code in C that was already written. We wrote a script in *Python* based on the library *subprocess* [30] which, basically, runs the C code and extracts the sensor's results. The code is demonstrated in appendix C.

The setup used for the optical power and temperature measurements is represented in figure 2.16 (schematic in figure 2.17).

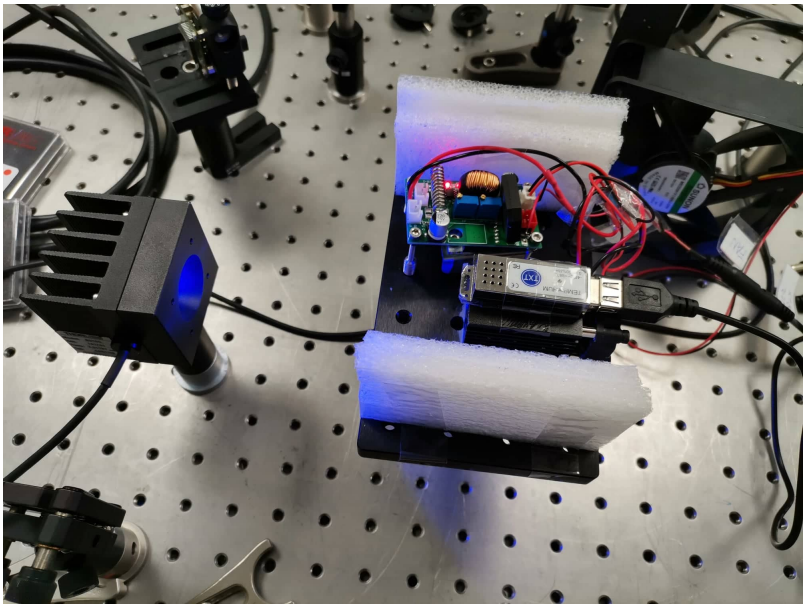

FIGURE 2.16: Setup used for the optical power and temperature measurements.

Having these *Python* scripts we just ran them simultaneously for 4 hours on the *Raspberry Pi*. The plots for both the optical power and the temperature of the laser as a function of time are represented in figure 2.18.

As we can see from the figure bellow the laser diode's optical power takes approximately 2000 seconds (33 minutes) to stabilize at around 2.435W. Also its temperature varies quite a bit even after the optical power stabilizes due to changes in the room's temperature and due to the entry and exit of people in the room. One should note that the temperature plot is only a reference and not the real diode's temperature because we could not measure it directly in the diode. The temperature sensor was in contact with the upper surface of the parallelepiped-shaped heat sink.

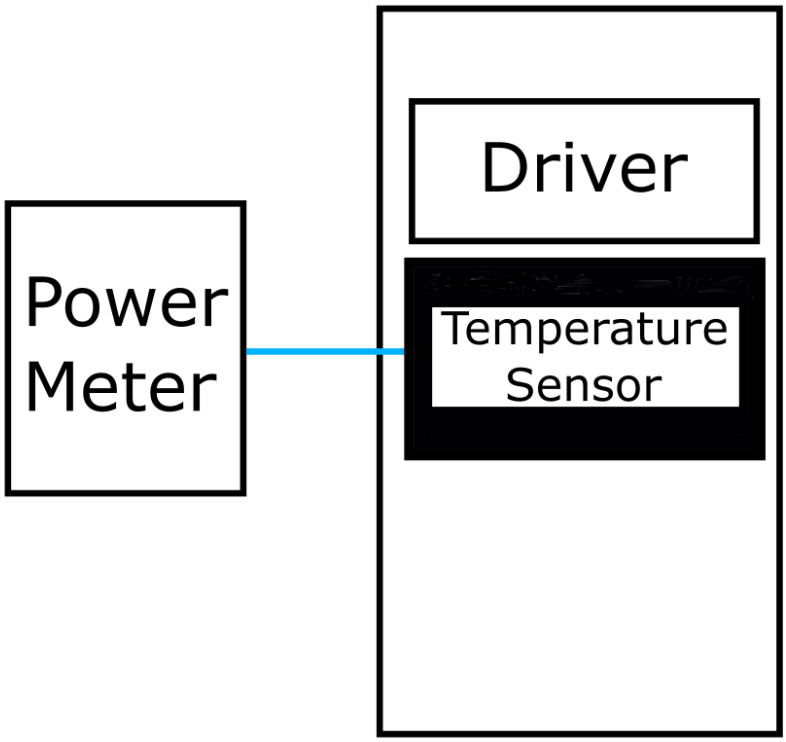


FIGURE 2.17: Schematic of the setup for measuring the optical power and the temperature of the laser as a function of time. Top view

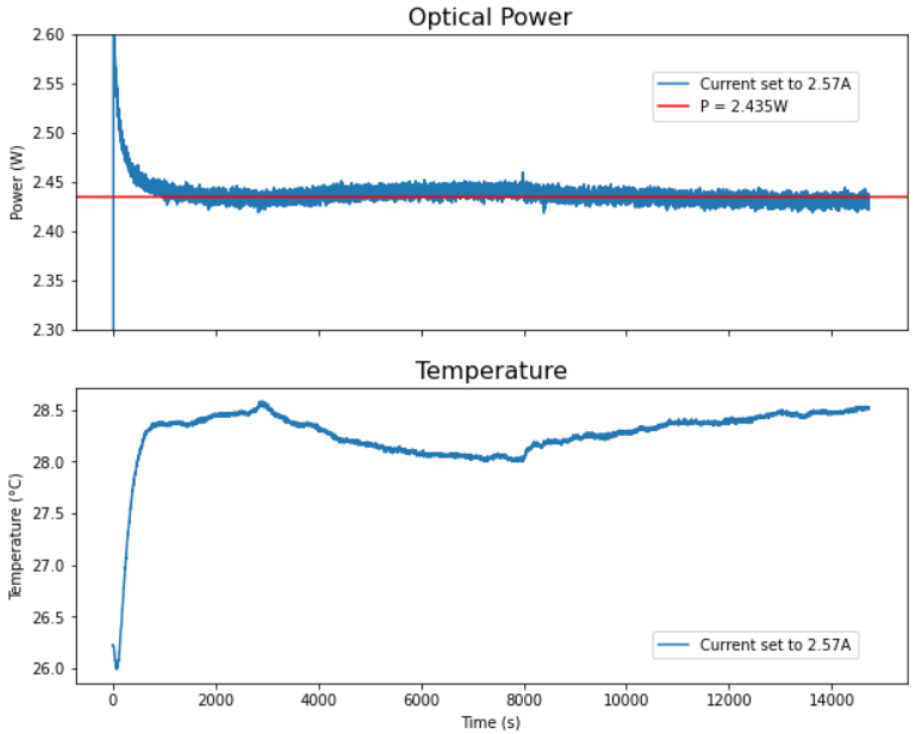


FIGURE 2.18: Measurements of the optical power and the temperature of the laser as a function of time.

We also measured the laser's spectrum with an *Avantes Starline AvaSpec-3648* spectrometer and the results are shown in figure 2.19.

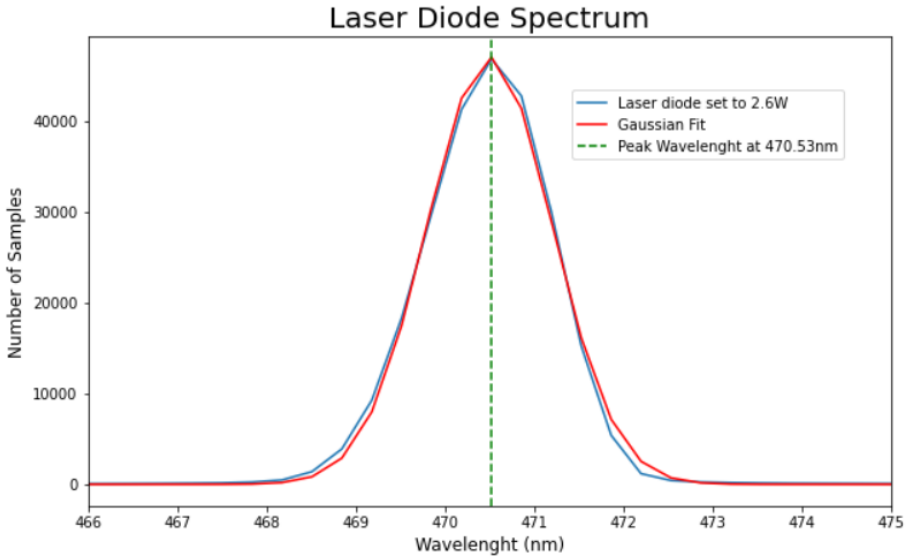


FIGURE 2.19: Laser diode's spectrum.

We can notice that the peak wavelenght is centered in 470 nm and that the curve's shape is very close to being a gaussian one. We can also see that the peak wavelenght is within the expected *Dominant Wavelength* specified in table 2.1.

## 2.6 $M^2$ measurements

### 2.6.1 Theoretical Background

As already discussed in subsection 1.3.1, knowing the laser beam's quality ($M^2$ *factor*) is crucial in the designing of a laser oscillator as it is the parameter that tells us how much is it possible for us to focus a beam. Recalling equation 1.29 we know that a diffraction-limited beam's spot size after a lens depends heavily on its diameter at the lens and on the focal length. In a Gaussian analysis we can easily modify equation 1.29 (and all the other Gaussian equations for the beam's propagation) by just substituting the wavelength by $M^2$ times the wavelength. Doing this we can also take into consideration beams that deviate from the ideal diffraction-limited Gaussian beams. With this modification equation 1.29 becomes:

$$w_{02} = \lambda f M^2 / \pi w_{01} \left[1 + \left(f / z_{R_1}\right)^2\right]^{1/2} \tag{2.1}$$

So an $M^2$ bigger than 1 (i.e., a beam that deviates from an ideal Gaussian one) will increase the spot size thus reducing the intensity of the beam and making it harder to pump the Ti:Sapphire oscillator. What we can do to compensate a beam with a higher $M^2$ *factor* is to either increase the beam's diameter at the lens or to choose one with a shorter focal length.

In order to calculate the $M^2$ *factor* we have to measure the radius of the beam along its propagation direction to obtain the graphical representation of the so called caustic. A problem that a more watchful reader may find lies within the definition of the beam's radius itself. In a Gaussian analysis the radius is defined, according to ISO Standard 11146, as the length to where the intensity drops to $1/e^2$ ($\approx$ 13.5%) of the value on the beam axis [31].

This concept of defining the beam's radius as the distance in the axis to where the intensity drops to $1/e^2$ can be applied to other profile shapes not being exclusive to Gaussian ones. The recommended definition, as already said, is the ISO Standard 11146 which is defined as:

$$w_i = 2\sqrt{\frac{\int x^2 I(x,y)dxdy}{\int I(x,y)dxdy}} \tag{2.2}$$

Where $i = x, y$, $I(x,y)$ is the intensity of the beam in a plane ortogonal to the direction of propagation, $z$, and $x^2$ is the horizontal coordinate. For a Gaussian profile equation 2.2 gives the same result as the $1/e^2$ method.

There are are numerous commercially available beam profilers which can automatically calculate the caustic for both the horizontal and vertical directions and its corresponding $M^2$ *factors*. In this work we did not have any of these systems so we used a CCD (Charge-Coupled Device) to measure the beam's radius and a ruler to measure the relative positions of the CCD and to keep it aligned.

### 2.6.2 Experimental Setup and Results

For measuring the $M^2$ *factor* we designed a setup in which we could operate at the optical power that we had intended to pump the Ti:Sapphire oscillator ($\approx$ 2.4W) and simultaneously use the CCD in front of the beam. This setup allowed us to visualize the beam's profile and not damaging the CCD. The schematic of the implemented setup is represented in figure 2.20:

W1 and W2 are glass wedges, M1 is a metallic mirror and we used an *IDS UI-2222SE-M* Charge-Coupled Device with an optical size of 6.374mm $\times$ 4.781mm and a pixel size

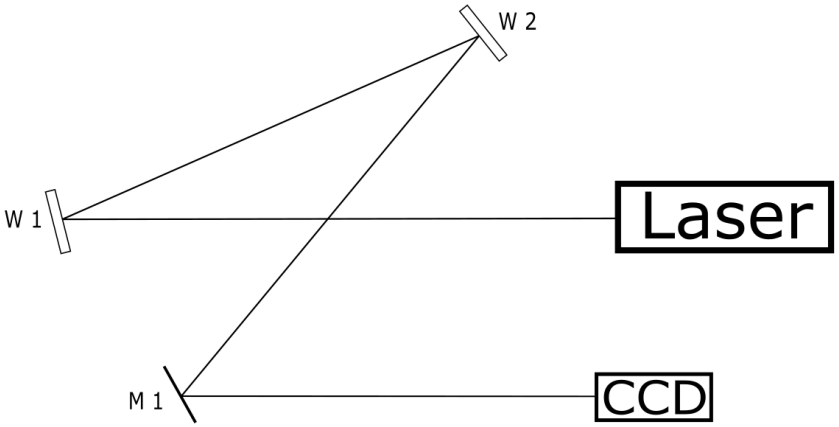


FIGURE 2.20: Scheme of the setup used for measuring the $M^2$ *factor*.

of 8.3$\mu$m $\times$ 8.3$\mu$m. The wedges were used to attenuate the beam (scheme represented in figure knowing that for small angles the reflectivity in glass is approximately 4% as represented in figure 2.21. We also made sure that we were using the first reflections

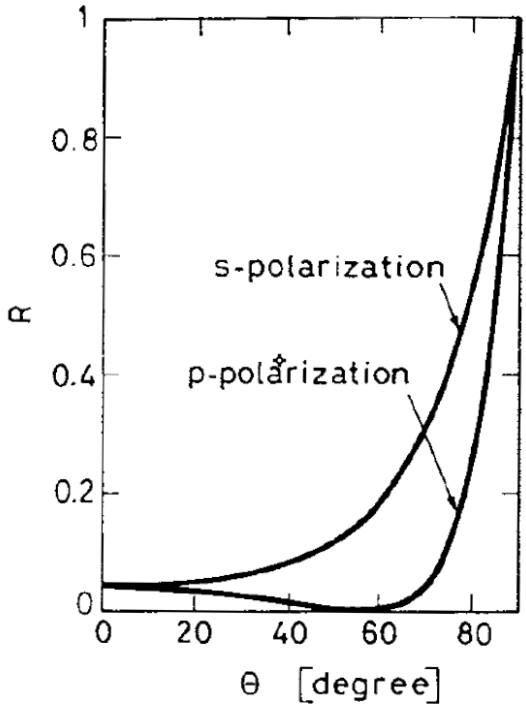


FIGURE 2.21: Reflectivity as a function of the angle of incidence in a glass interface [1].

at the air-glass interfaces and not the glass-air ones. Figure 2.22 illustrates this concept

better.

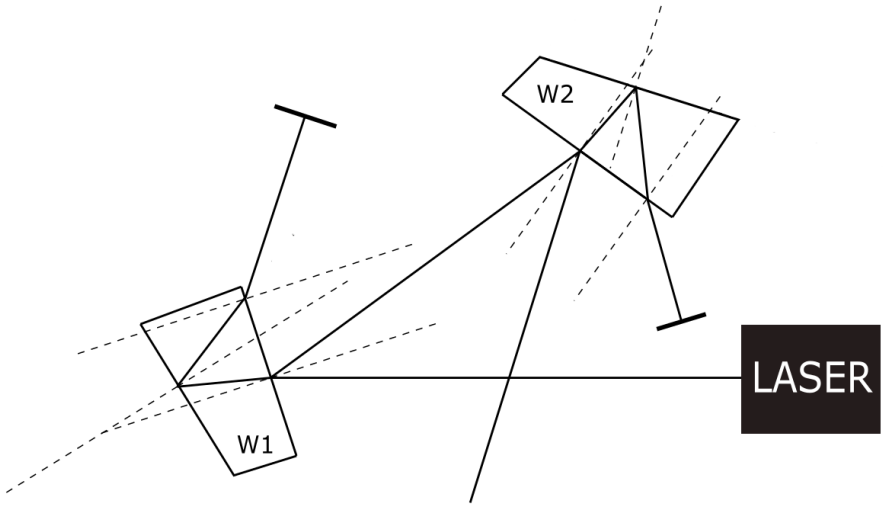


FIGURE 2.22: System of wedges.

In order to measure the beam's radius along its direction of propagation we used a ruler which also served as a way to keep the CCD aligned with the beam. The setup is represented in figure 2.23.

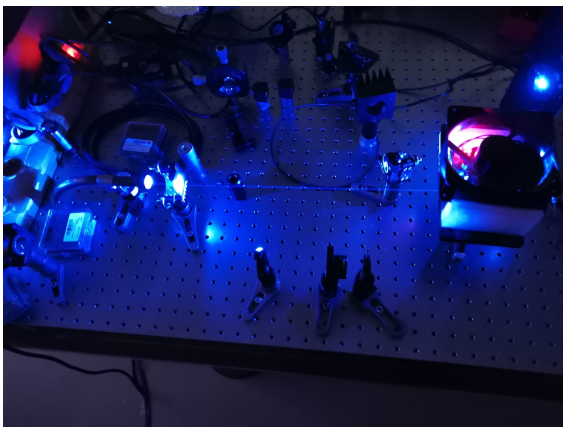

(A) Combination of wedges and a mirror.

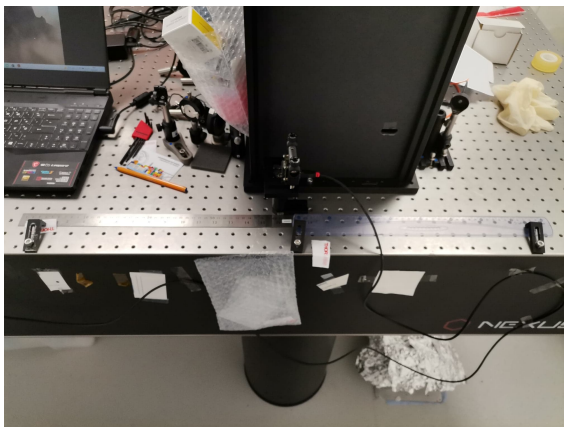

(B) Translation system for the CCD.

FIGURE 2.23: $M^2$ *factor* measurement setup.

Recalling figure 2.1 we see that the diode laser came preset with a positive lens that could not be removed. Just by turning on the laser diode we could notice that due to this lens the horizontal component of the beam converges and the vertical component diverges. We later measured the horizontal component's focus to be at 1.06m of distance from the source. In order to measure the $M^2$ *factor* of both the horizontal and the vertical

axis we focused the beam with a positive lens. The profiles of both axes are represented in figures 2.24 and 2.25:

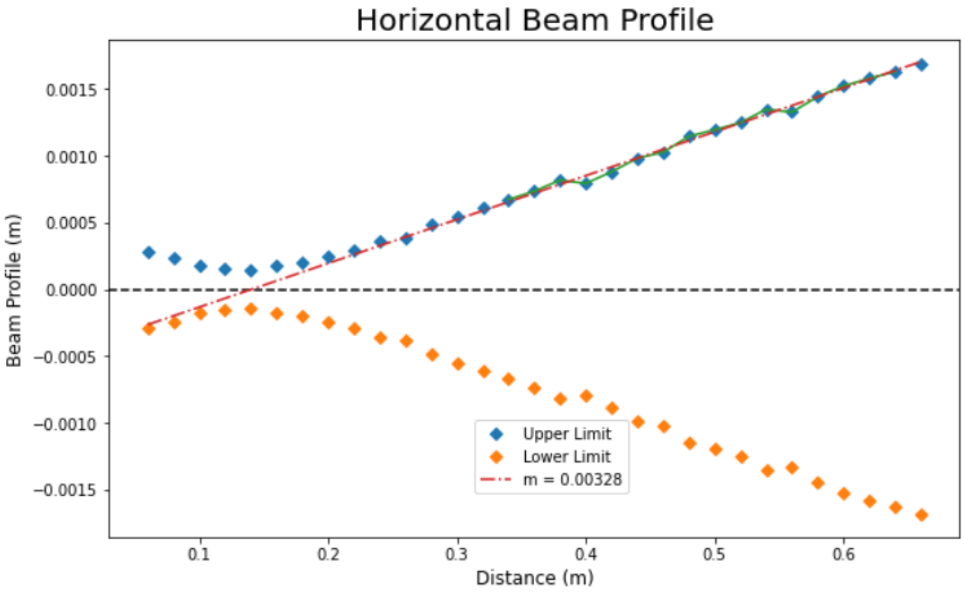


FIGURE 2.24: Evolution of the horizontal component's profile of the beam.

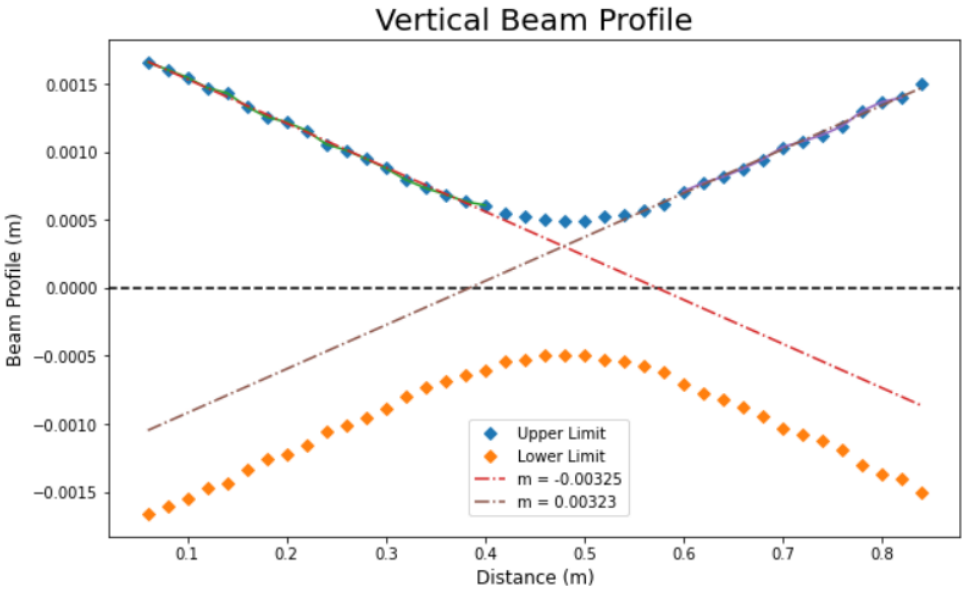


FIGURE 2.25: Evolution of the vertical component's profile of the beam.

With the *Python* function *min*, we calculated the vertical spot size, $w_{0v}$, to be 0.491 mm and the horizontal spot size, $w_{0h}$, to be 0.141 mm. Recalling equation 1.32 and knowing that the vertical divergence angle, $\theta_v$, and the horizontal one, $\theta_h$, are calculated (using the slope) by $\theta = \arctan(m)$, we calculated the $M^2$ *factor* for both axis to be $M_v^2 = 10.627$ and $M_h^2 = 3.010$.

We also measured the beam's divergence immediately at the exit of the laser diode with CCD and obtained, for the vertical axis, $\theta_v = 6.09$ mrad and, for the horizontal one, $\theta_h = -3.72$ mrad. The negative sign on the horizontal axis' divergence comes from the fact that this axis converges.

# Chapter 3

# Pumping of a Ti:Sapphire Oscillator

In this chapter we will be covering the collimation system designed for the blue laser diode as well as the experimental setup and procedures implemented for pumping the Ti:Sapphire oscillator.

## 3.1 Astigmatism Compensation and Collimation

Diode lasers are very astigmatic, *i.e.*, if we put a lens in front of the beam we will have two focal points (one behind the other), so it is necessary to correct it in order to use one to pump an oscillator. As already discussed primarily in section 1.3 and in section 2.6 the output beam of a laser diode is very divergent in both the horizontal and the vertical components and has $M^2$ *factors* way above 1. The most common way to compensate the astigmatism of a laser diode is to collimate one of the axes (usually the horizontal one which is the less diverging one) with an aspheric lens and to use a pair of cylindrical lenses in a telescopic configuration (either two positive lenses or one negative and one positive one) to expand the other axis. The astigmatism compensation comes from having this system set up so that the beam, after passing through it, is circularized, *i.e.*, both the vertical and the horizontal components with the same spatial dimensions.

In this work, since the laser's horizontal component diverges a lot ($\approx -3.72$ mrad as already discussed in section 2.6.2), we had to collimate it immediately at the exit of the laser to preserve its spatial dimension and than expand the vertical axis (divergence of $\approx 6.09$ mrad) so that at the exit of this system we had a circularized beam. This is essential for having the smallest possible spot size in the Ti:Sapphire crystal.

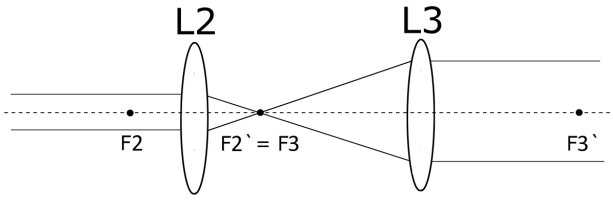


(A)

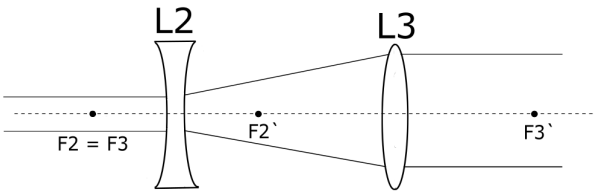


(B)

FIGURE 3.1: Pair of lenses in a telescopic configuration for expanding the vertical axis. (A) Telescopic configuration using two positive lenses; (B) Telescopic configuration using a combination of a negative and a positive lens.

For collimating the beam's **horizontal component** we considered the laser diode as a point source of light. In this framework and knowing that the beam's horizontal component is converging we just have to put in front of it a negative lens with its focal distance the same as the distance from the laser diode to where the beam focuses.

For expanding the beam's **vertical component** and than collimate it we just have to put a pair of lenses in a telescopic configuration (case represented in figure 3.1b). We can only do this if we put a negative cylindrical lens with an enough short focal distance so that the beam's divergence after it is much bigger than before it (at least one order of magnitude).

### 3.1.1 Simulations using the software *GaussianBeam*

We made some simulations using the software *GaussianBeam* and obtained a circularized beam with dimensions of $\approx$ 4mm $\times$ 4mm. This simulations are represented in figures 3.2 and 3.3.

Both the settings used on the software for the evolution of the horizontal and vertical profiles and the beam's characteristics are represented in table 3.1 and in table 3.2.

It should be noted that the software could only compute one component at a time.

FIGURE 3.2: Simulation performed with the software *GaussianBeam* for the beam's horizontal component.

FIGURE 3.3: Simulation performed with the software *GaussianBeam* for the beam's vertical component.

| Optics | Position (mm) | Properties | Waist ($\mu$m) | Divergence (mrad) |
|---|---|---|---|---|
| Beam | 0 | n = 1, $M^2$ = 3.73 | 4160 | -3.720 |
| Lens 1 | 4 | f = -1060 mm | 3924 | 0.142 |
| Lens 2 | 38 | n2/n1 = 1 | 3924 | 0.142 |
| Lens 3 | 171 | n2/n1 = 1 | 3924 | 0.142 |

TABLE 3.1: Settings used in the simulation of the evolution of the beam's horizontal profile.

| Optics | Position (mm) | Properties | Waist ($\mu$m) | Divergence (mrad) |
|---|---|---|---|---|
| Beam | 0 | n = 1, $M^2$ = 16 | 393 | 6.090 |
| Lens 1 | 4 | f = -1060mm | 391 | 6.124 |
| Lens 2 | 38 | f = -20mm | 88 | 27.209 |
| Lens 3 | 171 | f = 150mm | 4079 | 0.587 |

TABLE 3.2: Settings used in the simulation of the evolution of the beam's vertical profile.

Looking firstly at the evolution of the horizontal profile represented in figure 3.2 we can see two blocks of material at positions 38 and 171mm. This serves only to show that those are the positions of the cylindrical lenses and that they do not interfere with the evolution of the horizontal component of the beam. We wanted to preserve the waist's dimension at the laser diode (estimated to be $\approx$ 4160$\mu$m) so we chose a negative lens with a focal distance of -1060mm which is the distance from the laser diode to where the beam focuses and positioned the lens immediately in front of the laser diode. Both the divergence and the waist at the origin were the measured ones in section 2.6.2.

In the simulation of the evolution of the beam's vertical profile we knew that its dimension had to be around the same size as the horizontal one ($\approx$ 4160$\mu$m). In our simulations we found out that a combination of a negative cylindrical lens ($f = -20$mm) at 38mm from the origin and a positive cylindrical one ($f = 150$mm) at 171mm from the origin produced a collimated beam with a waist of 4079$\mu$m.

It should be noted that the choices of lenses were made taking into account off-the-shelf components. An infinite combination of lenses were possible but we did not want to custom-order more exotic lenses.

### 3.1.2 Implementation

With the simulations showing promising results we bought a negative meniscus lens with a focal length of -1000 mm (*Thorlabs LF1141-A*), a negative cylindrical lens with a focal length of -20.01 mm (*Thorlabs LK1085L1*) and a positive cylindrical lens with a focal length

of 150.00 mm (*Thorlabs LJ1934L1*). The lenses were placed according to the positions calculated on the simulations and the setup is represented in figure 3.4. Minor adjustments

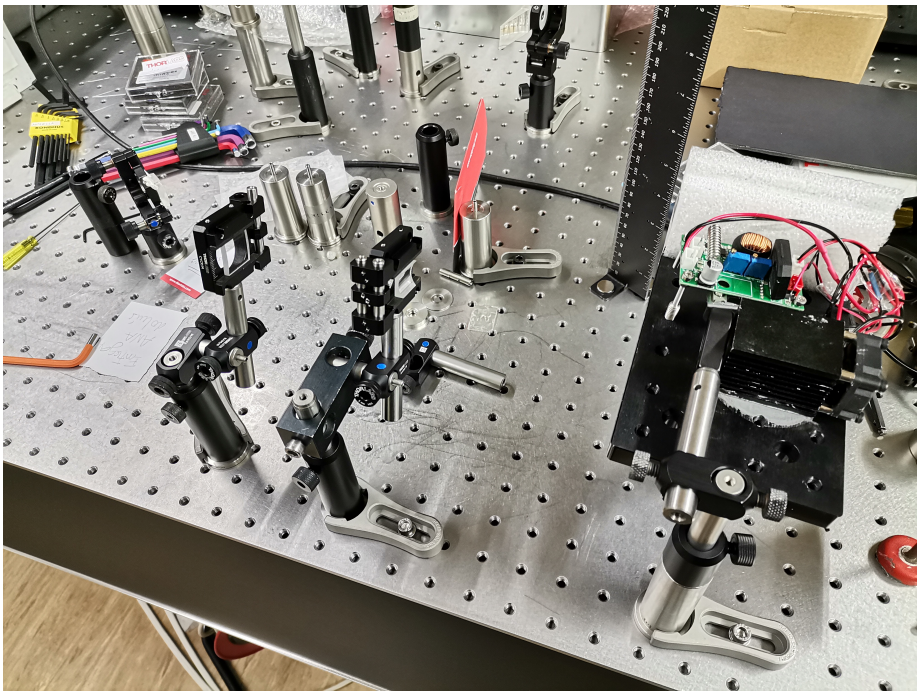

FIGURE 3.4: Combination of lenses used for expanding the beam's vertical profile and for collimation.

had to be made so that the beam was perfectly collimated with a diameter of $\approx 4 \times 4$ mm.

## 3.2 Experimental Setup and Results

A schematic of the Ti:Sapphire oscillator being pumped is represented in figure 3.5. From the figure below we can see: mirrors PM that are used to steer the beam; lens L that focuses the beam into the Ti:Sapphire crystal and is tilted to compensated for the fact that this crystal is cut in Brewster's angle; mirrors M1 and M2 form the cavity; the output coupler OC is where we have the output beam from the oscillator; mirrors DCM1, DCM2, DCM3 and DCM4 and the wedges W1 and W2 are used to compensate the dispersion of light pulses. This oscillator was optimized to operate in cw (continuous wave) mode of operation by tweaking the pump mirrors' positions until we reached the maximum output power for a steady pump power. Since we wanted to obtain the $P_{out}$ vs $P_{pump}$ graph for the laser diode being the pump source we firstly calculated the graph for the green DPSS (Diode-Pumped Solid-State) laser (*Coherent Verdi G7* with an $M^2$ *factor* of $\approx 1 \times 1$) being the pump source, represented in figure 3.5 (it should be noted that this oscillator was

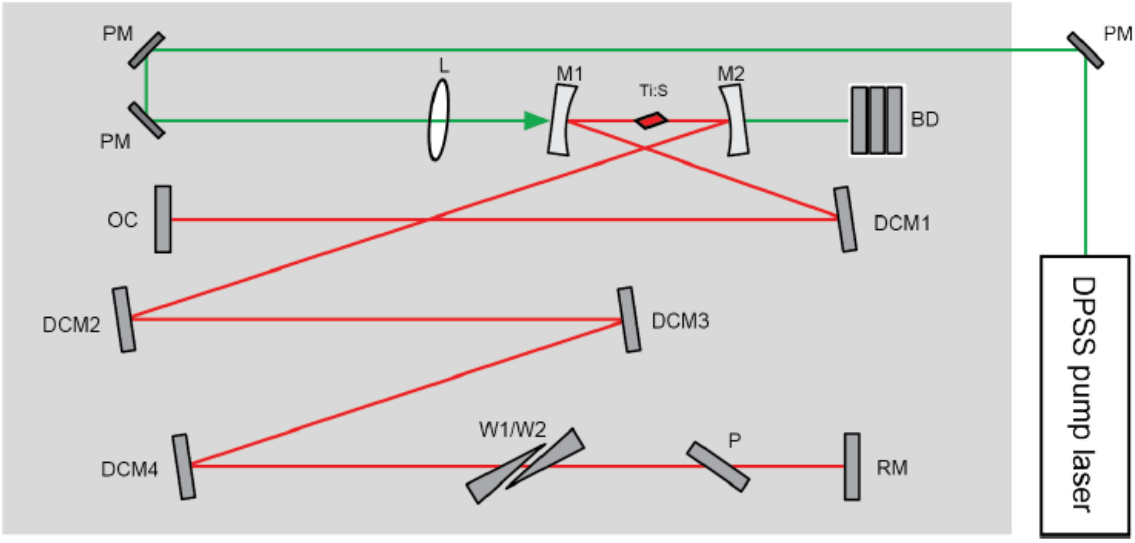


FIGURE 3.5: Ti:Sapphire being pumped [32]. *L* - lens; *M* - mirror; *PM* - pump mirror; *BD* - beam dump; *OC* - output coupler; *DCM* - double chirped mirror; *W* - wedge; *P* - $B_aF_2$ plate; *RM* - rear mirror.

designed for this DPSS laser which means that the pump mirrors were also designed for it - Wavelength range between 510 and 545 nm). The *Verdi G7*'s spectrum is represented in figure 3.6 and the graph obtained for the DPSS pump laser in figure 3.7:

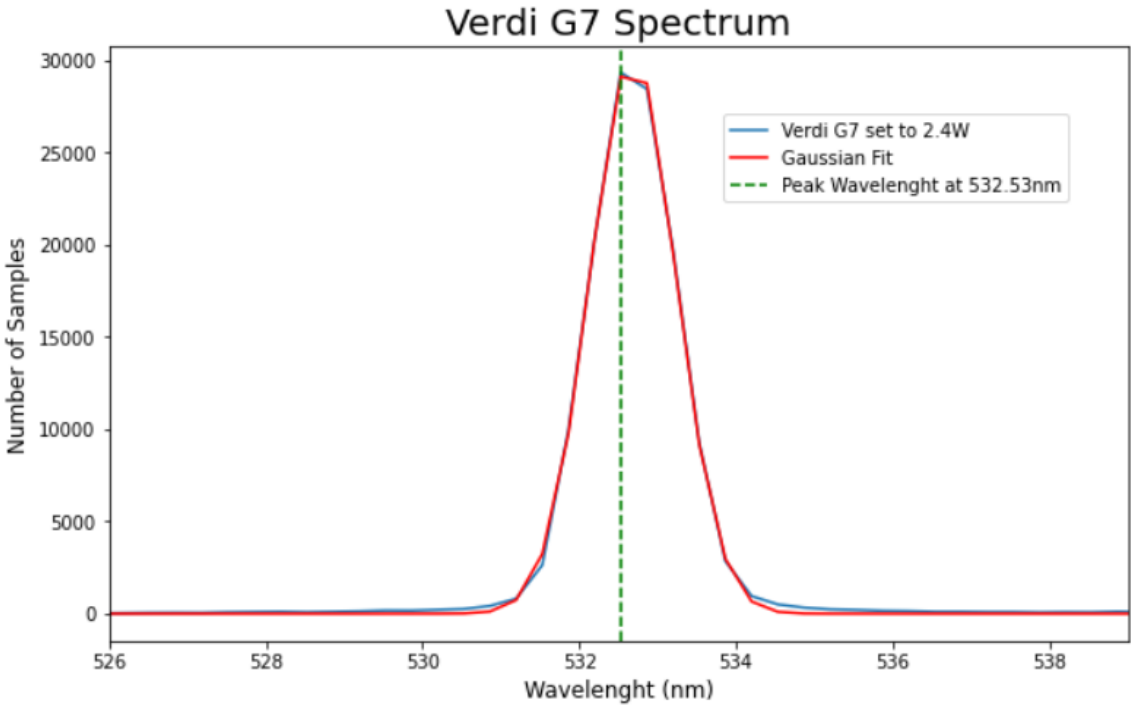


FIGURE 3.6: *Verdi G7*'s spectrum.

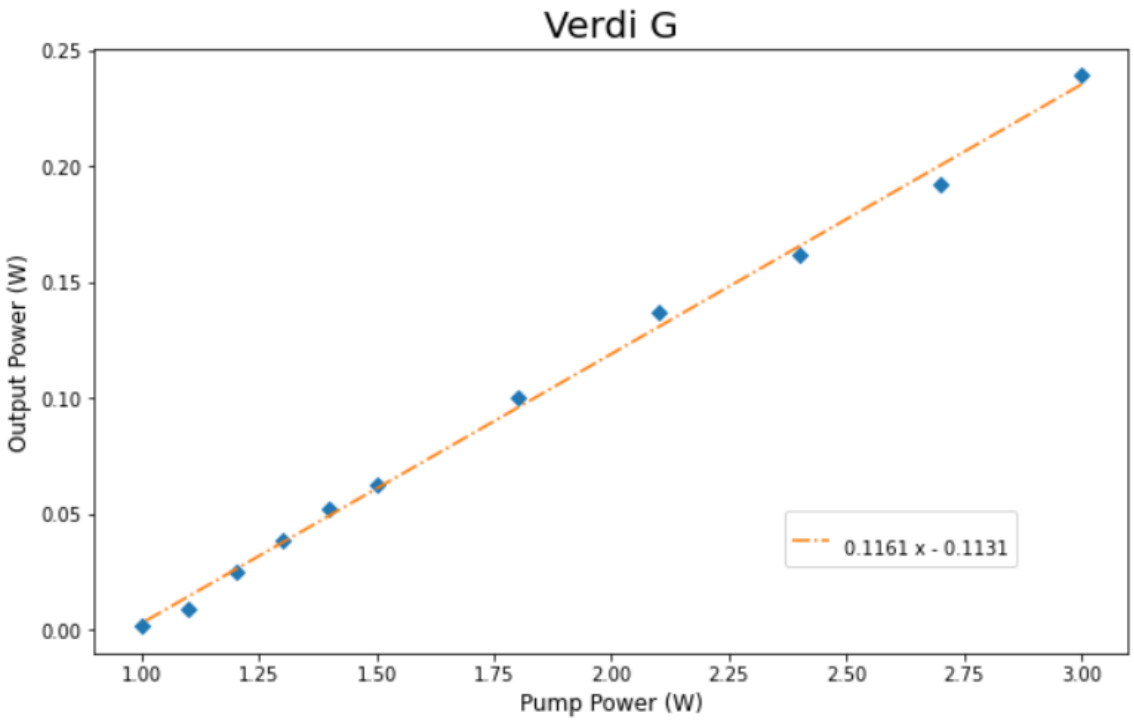


FIGURE 3.7: $P_{out}$ vs $P_{pump}$ graph for the DPSS pump laser (Verdi G).

From figure 3.7 we can see that laser emission from the oscillator starts at approximately 1 watt of pump power (using the DPSS pumping laser) and grows linearly with a slope efficiency of 0.12.

After pumping the Ti:Sapphire oscillator using the DPSS laser we substituted this one with the developed pump source based on our blue laser diode (it should be remembered that the laser diode has a maximum output optical power of 2.4 W). In order to do this we knew that we had to substitute all the pump mirrors, represented in figure 3.5 as PM, and mirrors M1 and M2 because these are designed to operate at 532 nm. We substituted the pump mirrors (PM as in figure 3.5) with new ones with a very high degree of reflectance for 470.53 nm. The graph of transmittance vs wavelength is represented in figure 3.8: PM_b represents the new pump mirrors and LD the laser diode. We can look more closely to the mirrors transmittance at 470.53 nm in figure 3.9:

We can see that the mirrors' transmittance is within 0 to 0.2%. Since these are dielectric mirrors, their absorbance is despicable which means that they have $\approx$ 99.8% reflectance and therefore they are very good to use with the blue diode. Unfortunately we could not get new mirrors M1 and M2 at the time of submission of this thesis and so we could not achieve continuous mode of operation with our blue laser diode. To find out why we were not succeeding we measured the optical power loss caused by poor transmission

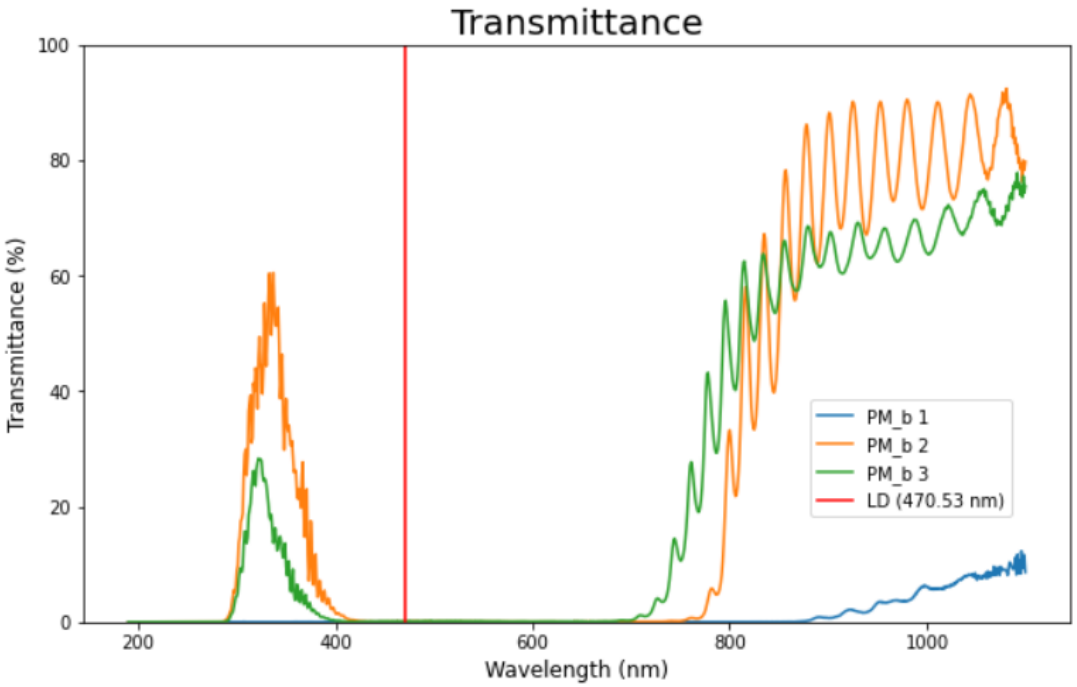


FIGURE 3.8: Transmittance versus wavelength for the new pump mirrors, PM1, PM2 and PM3. The transmittance was measured using a spectrophotometer.

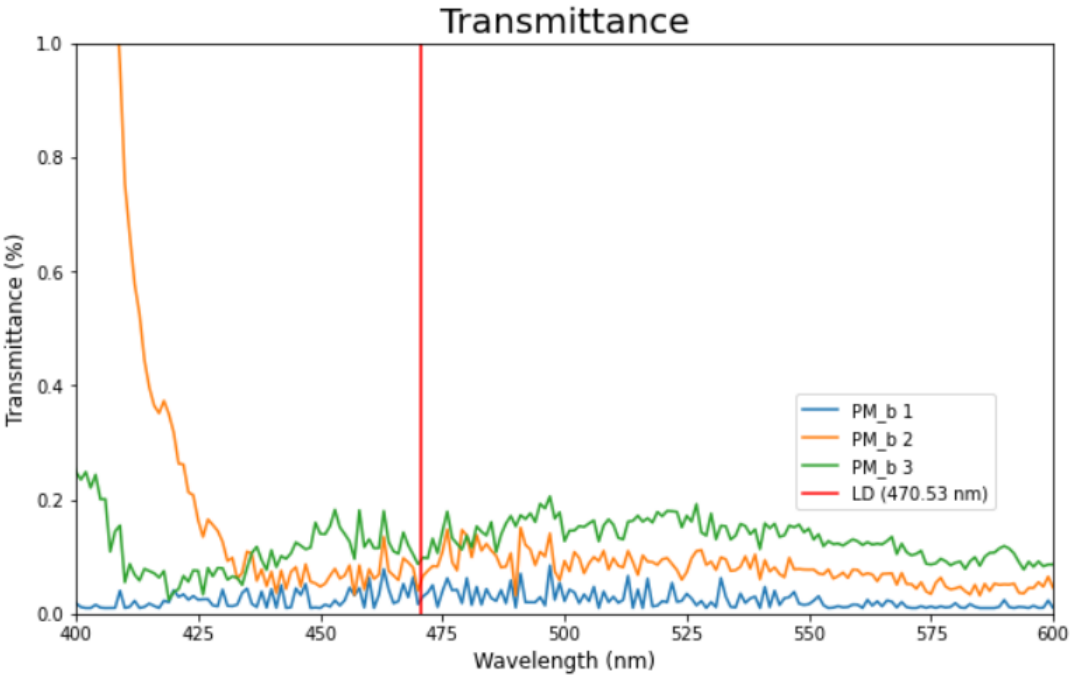


FIGURE 3.9: Mirrors' transmittance zoomed in.

from mirror M1. We found out that this mirror was blocking more than 40% of the optical power from reaching the crystal which represents a drop from 2.4W to less than 1.44W. It should be noted that, using the *Verdi G*, with 1.44W of optical power we could only achieve $\approx$ 50 mW.

We also tried to measure the beam's profile inside the crystal to find out if the lens, L, is well suited for our diode laser (from equation 1.29 we see that the spot size is smaller the smaller the focal length is). Since we had no space to place a CCD in the crystal's position and did not want to misalign the oscillator we measured the spot size for both pump sources (the DPSS laser and our blue laser diode) after collimating the beam with a focusing lens of with 60 cm of focal length, in order to calculate the scale factor and estimate the laser diode's behavior inside the crystal. These spot sizes are represented in figures 3.10 and 3.11:

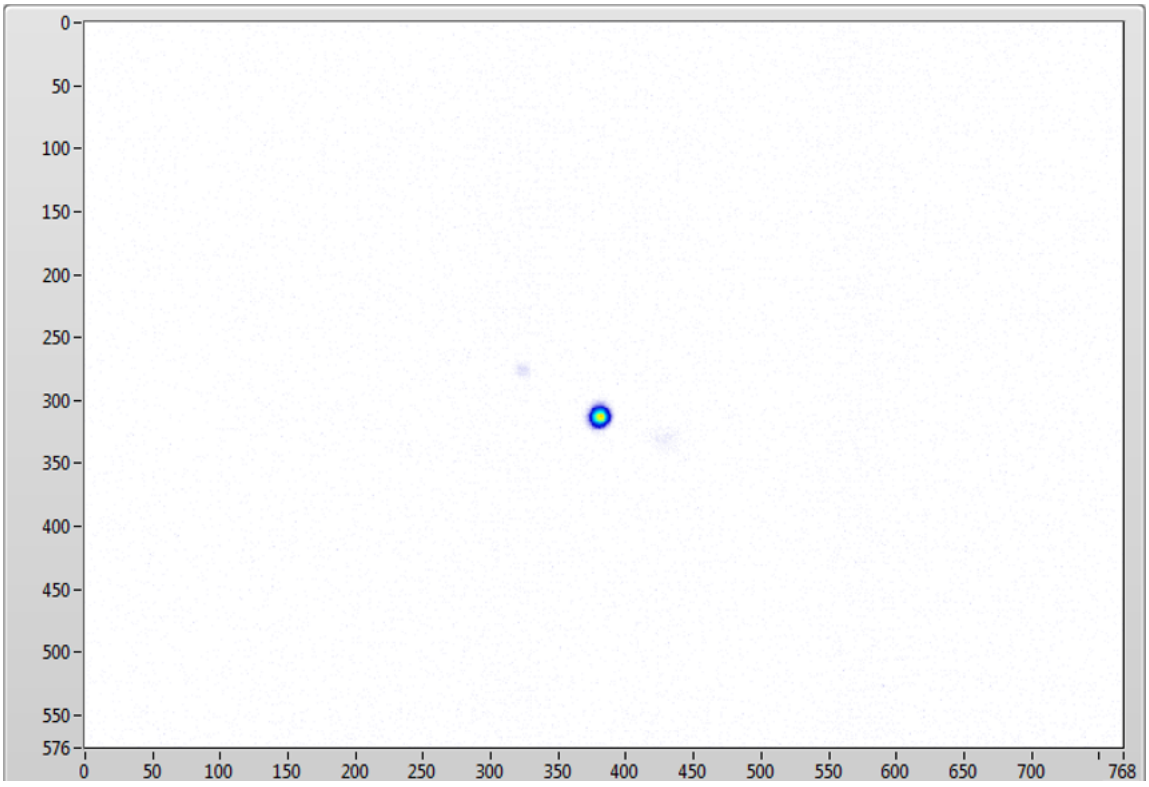


FIGURE 3.10: Verdi G's spot size after a lens with $f = 60$ cm. Both the horizontal and the vertical axis are in micrometers.

Using the software *ImageJ* we measured the area in pixels for both the spot sizes and found out that the blue laser diode's spot size is $\approx$ 8 times larger than the *Verdi G*'s (this means that when the blue laser diode's beam is focused in the crystal it will be 8 times larger that it should be, since the ideal dimensions are those of the Verdi G's). Not only

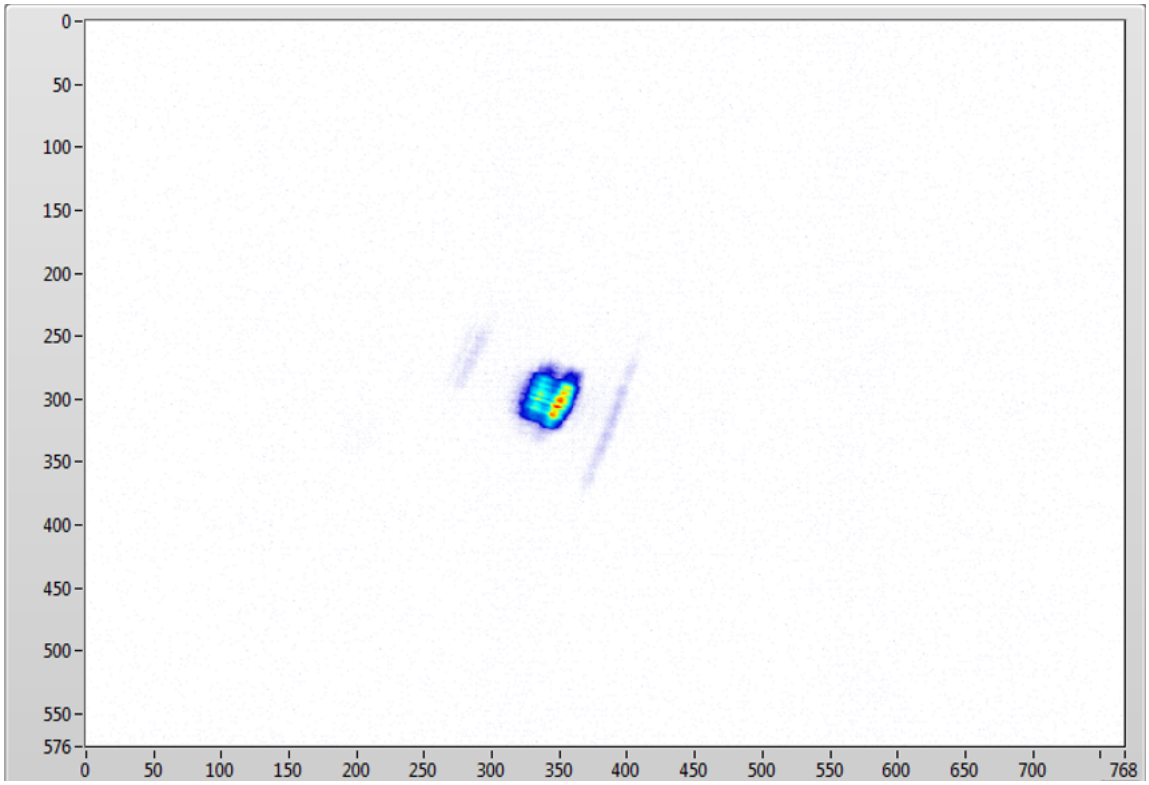


FIGURE 3.11: Blue laser diode's spot size after a lens with $f = 60$ cm. Both the horizontal and the vertical axis are in micrometers.

that the energy is more spread out across the beam's area whereas in the *Verdi G*'s one is more focused in the center. All this factors makes the laser diode's threshold pump power to be way higher than the *Verdi G*'s one.

# Chapter 4

# Final Remarks

In this thesis we have successfully built, characterized and designed a pump system for a Ti:Sapphire oscillator based on a blue laser diode (470 nm). This pump system is fully functional, having a stable output optical power and temperature and having the needed characteristics for pumping the oscillator namely having enough power, being collimated and being astigmatism-compensated.

In chapter 1 we oversaw the basic physical concepts needed for following along this thesis. We looked into the semiconductor laser operation, in particular the heterojunctions which are the basis of this devices, Gaussian beams which are a good approximation for this type of beams and the way these lasers behave when used as pump sources.

We fully dedicated chapter 2 for the complete characterization of the laser diode. We started by the characterization of the driver, measuring all the outputs and transients and then the assembly of the laser. This analysis includes the steps that we took for accomplishing good output and temperature stabilization as well as all the safety procedures that we took in order to safely handle the laser diode. We concluded that: the driver provided a smooth transient behavior and therefore was suited for diving the laser diode; the laser diode reaches 2.4 W of constant optical power.

Finally, chapter 3 is subdivided in two steps: the process of designing the collimation and astigmatism compensation system based on a combination of a meniscus lens and two cylindrical lenses in the telescopic configuration; the pumping of the Ti:Sapphire oscillator. We successfully built a beam-shaping system that after it our laser diode had $4 \times 4$ mm and was collimated. When pumping the oscillator we started by acquiring the $P_{out}$ vs $P_{pump}$ graph for the DPSS laser so that we could compare the laser diode's performance with a pump source that was already successfully being used. Unfortunately the

oscillator pump mirrors were designed for green light which makes our laser diode, for now, unusable as a pump source.

Nonetheless we already ordered a pair of pump mirrors designed for transmission at 470 nm that will arrive in a couple of weeks from the submission of this thesis. We are very confident that by substituting the pump mirrors with the new ones (and, if necessary, with further shaping of the beam) we will successfully pump the Ti:Sapphire oscillator. If this way of pumping is successful we are dealing with a huge cost reduction on pump sources since the typical DPSS lasers used as pump sources can cost two orders of magnitude more than these high power diode lasers.

# Appendix A

# *Nichia NUBM07E 465nm* datasheet

Bellow is represented the full datasheet of the *Nichia NUBM07E 465nm* laser diode:

***Blue Laser Diode Bank***

## *NUBM07E*

**Engineering Sample**

### ■Features

- High Power Multiple Laser Diode (LD) Bank
- 8 Collimator Beams
- No Outgas
- High Heat Dissipation
- High safety structure for prevention of removing LDs

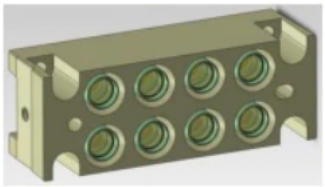

### ■Absolute Maximum Ratings

| Item | Symbol | Absolute Maximum Ratings | Unit |
|---|---|---|---|
| Forward Current (Tm=25°C ) | If | 3.5*1 | A |
| Allowable Reverse Current (Tm=25°C ) | Ir(LD) | 85*1 | mA |
| Storage Temperature | Tstg | -40 ~ 85 | °C |
| Operating Temperature | Tm | 0 ~ 65 | °C |

*1: Individual LD

### ■Initial Electrical/Optical Characteristics of LD Bank (Tm=25°C)

| Item | Condition | Symbol | Min | Typ. | Max | Unit |
|---|---|---|---|---|---|---|
| Optical Output Power | If=2.3A | Po | 20.7 | (23) | - | W |
| Dominant Wavelength | If=2.3A | λd | 460 | (465) | 470 | nm |
| Operating Voltage*2 | If=2.3A | Vop | 30 | - | 39 | V |
| Beam Pointing Tilt Angle*3 | If=2.3A | Δθ | - | - | 0.7 | deg |

*2: 8LDs series connection

*3: Beam Pointing Tilt Angle $\Delta\theta = \sqrt{\Delta\theta_{//}{}^2 + \Delta\theta_{\perp}{}^2}$ (Individual LD)

### ■Initial Electrical/Optical Characteristics of mounted LD (Tc=25°C)

| Item | | Condition | Symbol | Min | Typ. | Max | Unit |
|---|---|---|---|---|---|---|---|
| Optical Output Power | | If=2.3A | Po | - | (2.9) | - | W |
| Dominant Wavelength | | If=2.3A | λd | 458 | (465) | 472 | nm |
| Threshold Current | | CW | Ith | 300 | - | 550 | mA |
| Slope Efficiency | | CW | η | - | (1.6) | - | W/A |
| Operating Voltage | | If=2.3A | Vop | 3.7 | - | 4.9 | V |
| Beam Divergence*4 | Parallel | If=2.3A | θ// | 0.25 | (0.40) | 0.55 | deg |
| | Perpendicular | | θ⊥ | -0.8 | (0.1) | 0.8 | |

*4: Full angle at $1/e^2$ from peak intensity

FIGURE A.1: *Nichia NUBM07E 465nm* datasheet

# Appendix B

# Thorlabs PM100 *Python* code

```
import pyvisa as visa
import numpy as np
import matplotlib.pyplot as plt
from ThorlabsPM100 import ThorlabsPM100
import time

#print(pyvisa.ResourceManager().list_resources())       #This allows the user to
    know the device‘s USB code

rm = visa.ResourceManager()
inst = rm.open_resource('USB0::0x1313::0x8079::P1002410::INSTR')
power_meter = ThorlabsPM100(inst=inst)

itera    = 100
dt       = 1
y_axis   = np.zeros(itera)

for i in range(len(y_axis)):
    y_axis[i] = power_meter.read
    time.sleep(dt)

time = itera*dt
x_axis   = np.arange(0,time,dt)

plt.plot(x_axis, y_axis)
```

# Appendix C

# TEMPerHUM *Python* code

```
import numpy
import time
import subprocess

import os, sys
file_path1 = '/home/pi/8487-191F/ThorlabsPM100-1.2.2/ThorlabsPM100/'
sys.path.append(os.path.dirname(file_path1))
file_path2 = '/home/pi/8487-191F/PyVISA-py-0.5.2/pyvisa_py'
sys.path.append(os.path.dirname(file_path2))

print 'TEMPerHum 2 sensor Temperature Logging script'
print 'Saves to data to running folder, csv file with YYYYMMDD.csv name'

starttime = time.time()

cmd = ['sudo','/home/pi/temper/TEMPered1p2/utils/tempered']


while(1):

    p = subprocess.Popen(cmd,stdout=subprocess.PIPE,stderr=subprocess.PIPE)
    out, err = p.communicate()
    t0 = (time.time()-starttime)/60

    try:
```

```
26          r = out
            s0 = map(float,r.split(','))
28          if(len(s0) == 3):

30              T1 = s0[0]
                H1 = s0[1]
32              D1 = s0[2]
                P1 = power_meter.read
34              filename = "logs/"+time.strftime("%Y%m%d_temperature.csv")
                f = open(filename,"aw")
36              f.write("%5.4f,%2.2f,%2.2f,%2.2f\n"%(time.time(),T1,H1,D1,P1))
                f.close()
38              print("%5.4f,%2.2f,%2.2f,%2.2f"%(t0,T1,H1,D1,P1))
            else:
40              print(t0, ' - Invalid reading, Err:' , err.rstrip('\n'), 'Out:',out.
    rstrip('\n'))
        except:
42          print(t0, ' - Invalid reading, Err:' , err.rstrip('\n'))

44      time.sleep(10)
```

# Bibliography


[1] O. Svelto, *Principles of Lasers*. Springer US, 2010. [Online]. Available: https://books.google.pt/books?id=ioywRI5W2HEC [Cited on pages xiii, xiv, 1, 3, 4, 8, 9, 10, 15, 16, and 38.]

[2] W. W. Chow and S. W. Koch, *Semiconductor-laser fundamentals : physics of the gain materials*. New York: Springer, 1999. [Cited on page 1.]

[3] Wikimedia Commons. (2015) *Band Gap Comparison*. [Online]. Available: https://upload.wikimedia.org/wikipedia/commons/thumb/0/0b/Band_gap_comparison.svg/2000px-Band_gap_comparison.svg.png [Cited on pages xiii and 2.]

[4] A. Yariv and P. Yeh, *Photonics: Optical Electronics in Modern Communications (The Oxford Series in Electrical and Computer Engineering)*. USA: Oxford University Press, Inc., 2006. [Cited on pages xiii, 7, and 8.]

[5] R. P. Encyclopedia. Laser diodes. [Online]. Available: https://www.rp-photonics.com/laser_diodes.html [Cited on pages xiii and 9.]

[6] F. L. Pedrotti, L. M. Pedrotti, and L. S. Pedrotti, *Introduction to Optics*, 3rd ed. Cambridge University Press, 2017. [Cited on pages xiii and 12.]

[7] Wikipedia. Gaussian beam. [Online]. Available: https://en.wikipedia.org/wiki/Gaussian_beam [Cited on pages xiii and 12.]

[8] A. E. Siegman, *Lasers*. University Science Books, 1986. [Cited on page 13.]

[9] P. W. Roth, A. J. Maclean, D. Burns, and A. J. Kemp, "Directly diode-laser-pumped ti:sapphire laser," *Opt. Lett.*, vol. 34, no. 21, pp. 3334–3336, Nov 2009. [Online]. Available: http://ol.osa.org/abstract.cfm?URI=ol-34-21-3334 [Cited on page 13.]

[10] S. Nakamura, M. Senoh, S. ichi Nagahama, N. Iwasa, T. Yamada, T. Matsushita, H. Kiyoku, and Y. Sugimoto, "InGaN-based multi-quantum-well-structure laser diodes," *Japanese Journal of Applied Physics*, vol. 35, no. Part 2, No. 1B, pp. L74–L76, jan 1996. [Online]. Available: https://doi.org/10.1143/jjap.35.l74 [Cited on page 13.]

[11] P. W. Roth, A. J. Maclean, D. Burns, and A. J. Kemp, "Direct diode-laser pumping of a mode-locked ti:sapphire laser," *Opt. Lett.*, vol. 36, no. 2, pp. 304–306, Jan 2011. [Online]. Available: http://ol.osa.org/abstract.cfm?URI=ol-36-2-304 [Cited on page 13.]

[12] H. Liu, G. Wang, J. Jiang, W. Tian, D. Zhang, H. Han, S. Fang, J. Zhu, and Z. Wei, "Sub-10-fs pulse generation from a blue laser-diode-pumped ti:sapphire oscillator," *Chin. Opt. Lett.*, vol. 18, no. 7, p. 071402, Jul 2020. [Online]. Available: http://col.osa.org/abstract.cfm?URI=col-18-7-071402 [Cited on pages 14, 18, and 21.]

[13] Olympus - Life Science Solutions. Ti:sapphire mode-locked lasers. [Online]. Available: https://www.olympus-lifescience.com/en/microscope-resource/primer/java/lasers/tsunami/ [Cited on pages xiii and 14.]

[14] R. P. Encyclopedia. Broad area laser diodes. [Online]. Available: https://www.rp-photonics.com/broad_area_laser_diodes.html [Cited on pages xiii and 14.]

[15] C. Engineering. Diode pumped lasers overview. [Online]. Available: http://www.aml.engineering.columbia.edu/ntm/level3/ch02/html/l3c02s01.html [Cited on pages xiii and 17.]

[16] S. Backus, M. Kirchner, C. Durfee, M. Murnane, and H. Kapteyn, "Direct diode-pumped kerr lens 13 fs ti:sapphire ultrafast oscillator using a single blue laser diode," *Opt. Express*, vol. 25, no. 11, pp. 12 469–12 477, May 2017. [Online]. Available: http://www.opticsexpress.org/abstract.cfm?URI=oe-25-11-12469 [Cited on pages 18 and 21.]

[17] D. A. Kopylov, M. N. Esaulkov, I. I. Kuritsyn, A. O. Mavritskiy, B. E. Perminov, A. V. Konyashchenko, T. V. Murzina, and A. I. Maydykovskiy, "Kerr-lens mode-locked ti:sapphire laser pumped by a single laser diode," *Laser Physics Letters*, vol. 15, no. 4, p. 045001, feb 2018. [Online]. Available: https://doi.org/10.1088/1612-202x/aaa62a [Cited on pages 18 and 21.]

[18] N. Sugiyama, H. Tanaka, and F. Kannari, "Mode-locked ti:sapphire laser oscillators pumped by wavelength-multiplexed laser diodes," *Japanese Journal of Applied Physics*, vol. 57, no. 5, p. 052701, mar 2018. [Online]. Available: https://doi.org/10.7567/jjap.57.052701 [Cited on page 18.]

[19] P. Castro-Marin, T. Mitchell, J. Sun, and D. T. Reid, "Characterization of a carrier-envelope-offset-stabilized blue- and green-diode-pumped ti:sapphire frequency comb," *Opt. Lett.*, vol. 44, no. 21, pp. 5270–5273, Nov 2019. [Online]. Available: http://ol.osa.org/abstract.cfm?URI=ol-44-21-5270 [Cited on page 21.]

[20] A. Muti, A. Kocabas, and A. Sennaroglu, "5-nJ femtosecond ti3+:sapphire laser pumped with a single 1 w green diode," *Laser Physics Letters*, vol. 15, no. 5, p. 055302, apr 2018. [Online]. Available: https://doi.org/10.1088/1612-202x/aaaea7 [Cited on page 21.]

[21] K. Gurel, V. J. Wittwer, M. Hoffmann, S. Schilt, and T. Sudmeyer, "Diode-pumped kerr-lens modelocked ti:sapphire laser generating 450 mw in 58 fs pulses and 350 mw in 39 fs pulses," in *Advanced Solid State Lasers*. Optical Society of America, 2015, p. ATh4A.8. [Online]. Available: http://www.osapublishing.org/abstract.cfm?URI=ASSL-2015-ATh4A.8 [Cited on page 21.]

[22] K. Gurel, V. J. Wittwer, M. Hoffmann, C. J. Saraceno, S. Hakobyan, B. Resan, A. Rohrbacher, K. Weingarten, S. Schilt, and T. Sudmeyer, "Green-diode-pumped femtosecond ti:sapphire laser with up to 450 mw average power," *Opt. Express*, vol. 23, no. 23, pp. 30 043–30 048, Nov 2015. [Online]. Available: http://www.opticsexpress.org/abstract.cfm?URI=oe-23-23-30043 [Cited on page 21.]

[23] R. Sawada, H. Tanaka, N. Sugiyama, and F. Kannari, "Wavelength-multiplexed pumping with 478- and 520-nm indium gallium nitride laser diodes for ti:sapphire laser," *Appl. Opt.*, vol. 56, no. 6, pp. 1654–1661, Feb 2017. [Online]. Available: http://ao.osa.org/abstract.cfm?URI=ao-56-6-1654 [Cited on page 21.]

[24] S. Sawai, A. Hosaka, H. Kawauchi, K. Hirosawa, and F. Kannari, "Demonstration of a ti:sapphire mode-locked laser pumped directly with a green diode laser," *Applied Physics Express*, vol. 7, no. 2, Feb. 2014. [Cited on page 21.]

[25] W. G. Olsen, D. J. Hodgson, and B. D. Bowen, "A standard for measuring transient suppression of laser diode drivers," *ILX Lightwave Corp.*, pp. 2–7, mar 2003. [Cited on pages 26 and 32.]

[26] L. A. Johnson, "Controlling temperatures of diode lasers and detectors thermoelectrically," 2003. [Cited on page 27.]

[27] I. RPMC Lasers. 12 do's and don'ts for laser diodes. [Online]. Available: https://blog.rpmclasers.com/12-dos-and-donts-for-laser-diodes [Cited on page 31.]

[28] PyPI. Thorlabspm100 1.2.2. [Online]. Available: https://pypi.org/project/ThorlabsPM100/ [Cited on page 34.]

[29] PyPI. Pyvisa 1.11.3. [Online]. Available: https://pypi.org/project/PyVISA/ [Cited on page 34.]

[30] Python. subprocess — subprocess management. [Online]. Available: https://docs.python.org/3/library/subprocess.html [Cited on page 34.]

[31] R. P. Encyclopedia. Beam radius. [Online]. Available: https://www.rp-photonics.com/beam_radius.html [Cited on page 37.]

[32] R. Ferreira, "Few-cycle laser for real-time nanomedicine research," Master's thesis, Faculdade de Ciências da Universidade do Porto, 7 2018. [Cited on pages xiv and 48.]